

Motion of grain boundaries incorporating dislocation structure

Luchan Zhang^a, Yang Xiang^{a,*}

^a*Department of Mathematics, The Hong Kong University of Science and Technology, Clear Water Bay, Kowloon, Hong Kong*

Abstract

In this paper, we present a continuum model for the dynamics of low angle grain boundaries in two dimensions incorporating both the motion of grain boundaries and the dislocation structure evolution on the grain boundaries. This model is derived from the discrete dislocation dynamics model. The long-range elastic interaction between dislocations is included in the continuum model, which ensures that the dislocation structure on a grain boundary is consistent with the Frank's formula. These evolutions of the grain boundary and its dislocation structure are able to describe both normal motion and tangential translation of the grain boundary and grain rotation due to both coupling and sliding. Since the continuum model is based upon dislocation structure, it naturally accounts for the grain boundary shape change during the motion and rotation of the grain boundary by motion and reaction of the constituent dislocations. Using the derived continuum grain boundary dynamic model, simulations are performed for the dynamics of circular and non-circular two dimensional grain boundaries, and the results are validated by discrete dislocation dynamics simulations.

Keywords: Grain boundary dynamics; dislocation dynamics; long-range elastic interaction; grain rotation; coupling and sliding

1. Introduction

Grain boundaries are the interfaces of grains with different orientations and play essential roles in the polycrystalline materials (Sutton and Balluffi, 1995). Grain boundaries migrate

*Corresponding author

Email address: maxiang@ust.hk (Yang Xiang)

under various driving forces such as the capillarity force, the bulk energy difference, the concentration gradients across the boundary, and the applied stress field. The motion of grain boundaries crucially determines the mechanical and plastic behaviors of materials. The classical grain boundary dynamics models are based upon the motion by mean curvature to reduce the total interfacial energy (Herring, 1951; Mullins, 1956; Sutton and Balluffi, 1995) using the misorientation-dependent grain boundary energy (Read and Shockley, 1950). There are extensive studies in the literature on such motion of grain boundaries by using molecular dynamics or continuum simulations, e.g. (Chen and Yang, 1994; Upmanyu et al., 1998; Kobayashi et al., 2000; Kazaryan et al., 2000; Upmanyu et al., 2002; Zhang et al., 2005; Upmanyu et al., 2006; Kirch et al., 2006; Elsey et al., 2009; Lazar et al., 2010; Esedoglu, 2016).

It has been shown that the grain boundary normal motion can induce a coupled tangential motion which is proportional to the normal motion, as a result of the geometric constraint that the lattice planes must be continuous across the grain boundary (Li et al., 1953; Srinivasan and Cahn, 2002; Cahn and Taylor, 2004). Besides the tangential motion coupled with normal motion, there is another type of tangential motion that is the relative rigid-body translation of the grains along the boundary by sliding to reduce the grain boundary energy (Li, 1962; Harris et al., 1998; Kobayashi et al., 2000; Upmanyu et al., 2006; Esedoglu, 2016). When a grain is embedded in another one, the tangential motions along a grain boundary give rise to a relative rotation between the two grains, leading to change of the misorientation of the grain boundary. In the grain rotation due to sliding, the misorientation angle goes to the nearby local energy minimum state (decreases for a low angle grain boundary), whereas in the grain rotation due to coupling, the misorientation angle increases.

Cahn and Taylor (Cahn and Taylor, 2004; Taylor and Cahn, 2007) formulated the phenomena of the coupling and sliding associated with the grain boundary motion. The tangential velocity induced by coupling effect is proportional the normal velocity v_{\perp} with the coupling parameter β , and the tangential velocity produced by sliding effect is v_s . Accordingly, the total tangential velocity v_{\parallel} is the superposition of these two effect: $v_{\parallel} = \beta v_{\perp} + v_s$.

They discussed different cases for the rotation of a circular cylindrical grain embedded in another one (Cahn and Taylor, 2004). When the grain does not have such symmetry, they proposed a generalized theory based on mass transfer by diffusion confined on the grain boundary (Taylor and Cahn, 2007).

Molecular dynamics simulations have been performed to validate the theory of Cahn and Taylor on the coupling grain boundary motion to shear deformation for planar grain boundary (Cahn et al., 2006b,a), and grain boundary migration and grain rotation for closed circle cylindrical grain boundaries (Srinivasan and Cahn, 2002; Trautt and Mishin, 2012). Experimental observations have also been reported on the migration of low angle planar tilt boundaries coupled to shear deformation in Al bicrystal with stress (Molodov et al., 2007; Gorkaya et al., 2009). The ratios of the normal to the lateral motion that they measured are complied with the coupling factors in the theory and atomistic simulations by Cahn *et al* (Cahn and Taylor, 2004; Cahn et al., 2006b,a). Phase field crystal model (an atomistic-level model) was employed to simulate the dynamics of a two-dimensional circular grain, and grain rotation and translation by motion and reaction of the constituent dislocations were observed (Wu and Voorhees, 2012). Phase field crystal simulations also showed that the coupling of grain boundary motion in polycrystalline systems can give rise to a rigid body translation of the lattice as a grain shrinks and that this process is mediated by dislocation climb and dislocation reactions (McReynolds et al., 2016). Three-dimensional phase field crystal simulations were further performed to investigate the motion, rotation and dislocation reactions on a spherical grain in a BCC bicrystal (Yamanaka et al., 2017). Numerical simulations based upon the generalization of the Cahn-Taylor theory to noncircular grains (Taylor and Cahn, 2007) were performed using the level set method (Basak and Gupta, 2014).

In this paper, we present a continuum model for the dynamics of low angle grain boundaries in two dimensions incorporating both the motion of grain boundaries and the dislocation structure evolution on the grain boundaries (Eqs. (16) and (17) in Sec. 3). The long-range elastic interaction between dislocations is included in the continuum model, which ensures that the dislocation structures on the grain boundaries are consistent with the

Frank's formula for grain boundaries (the condition of cancellation of the far-field elastic fields). These evolutions of the grain boundary and its dislocation structure are able to describe both normal motion and tangential translation of grain boundaries and grain rotation due to both coupling and sliding effects. Since the continuum model is based upon dislocation structure, it naturally accounts for the grain boundary shape change during the motion and rotation of the grain boundary by motion and reaction of the constituent dislocations without explicit mass transfer. Our model can be considered as a generalization of the Cahn-Taylor theory (Cahn and Taylor, 2004) by incorporating detailed formulas of the driving forces for the normal and tangential grain boundary velocities that depend on the constituent dislocations, their Burgers vectors, and the grain boundary shape, as well as the shape change of the grain boundaries, and is different from their earlier generalization based on mass transfer via surface diffusion (Taylor and Cahn, 2007). Note that in some existing continuum models for the motion of grain boundaries and grain rotation (Li, 1962; Kobayashi et al., 2000; Upmanyu et al., 2006; Esedoglu, 2016), evolution of misorientation angle was included to reduce the grain boundary energy density, which are able to capture the grain boundary sliding but not coupling. In our continuum model, we use dislocation densities on the grain boundary as variables instead of the misorientation angle, which enables the incorporation both the grain boundary coupling and sliding motions. Using the derived continuum grain boundary dynamic model, simulations are performed for the dynamics of circular and non-circular two dimensional grain boundaries. We also perform discrete dislocation dynamics simulations for the dynamics of these grain boundaries and the simulation results using the two models agree excellently with each other. In particular, both our continuum and discrete dislocation dynamics simulations show that without dislocation reaction, a non-circular grain boundary shrinks in a shape-preserving way due to the coupling effect, which is consistent with the prediction of the continuum model in Taylor and Cahn (2007) based on mass transfer via surface diffusion.

Our continuum grain boundary dynamics model is based upon the continuum framework for grain boundaries in Zhu and Xiang (2014) derived rigorously from the discrete dislocation dynamics model. Previously, a continuum model for the energy and dislocation structures

on static grain boundaries has been developed (Zhang et al., 2017a) using this framework. In fact, the energetic and dynamic properties of grain boundaries were understood based on the underlying dislocation mechanisms in many of the available theories, simulations and experiments (Read and Shockley, 1950; Li et al., 1953; Srinivasan and Cahn, 2002; Cahn and Taylor, 2004; Cahn et al., 2006b,a; Molodov et al., 2007; Gorkaya et al., 2009; Trautt and Mishin, 2012; Wu and Voorhees, 2012; McReynolds et al., 2016; Yamanaka et al., 2017). Although direct discrete dislocation dynamics simulations are able to provide detailed information of grain boundary or interface structures and dynamics (Lim et al., 2009; Quek et al., 2011; Lim et al., 2012), continuum models of the dynamics of grain boundaries incorporating their dislocation structures are still desired for larger scale simulations without tracking individual dislocations.

The rest of the paper is organized as follows. In Sec. 2, we describe the two dimensional settings of the grain boundaries with their dislocation structures, and review the continuum framework in Zhu and Xiang (2014) based on which our continuum model will be developed. In Sec. 3, we present our continuum model for the motion of grain boundaries. The variational derivation method of the continuum model is presented in the Appendix. In Sec. 4, we discuss the calculation of the misorientation angle based on the Frank's formula, which is maintained by the long-range dislocation interaction of the grain boundary during its motion. In Sec. 5, we present the formula for the change of misorientation angle (grain rotation) derived from our continuum dynamics model. We also derive the formulas for the tangential motions of grain boundaries due to the coupling and sliding effects based on our continuum model, and make comparisons with the formulas in the Cahn-Taylor theory (Cahn and Taylor, 2004; Trautt and Mishin, 2012). Simulation results for the dynamics of circular and non-circular two dimensional grain boundaries using our continuum model and comparisons with discrete dislocation dynamics simulation results are presented in Sec. 6. Conclusions and discussion are made in Sec. 7.

2. Grain boundaries in two dimensions and review of the continuum framework in Zhu and Xiang (2014)

We consider the two dimensional problem that one cylindrical grain is embedded in another grain with arbitrary cross-section shape. The inner grain has a misorientation angle θ relative to the outer grain, and the rotation axis is parallel to the cylindrical axis. The grain boundary is then a pure tilt boundary.

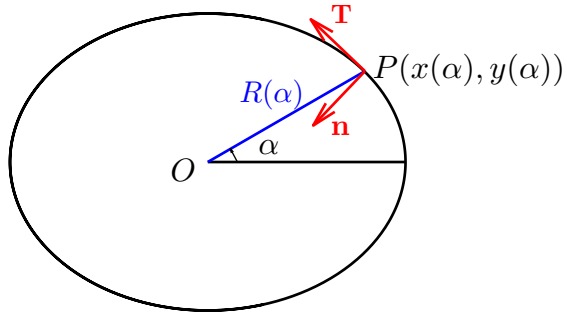


Figure 1: The cross-section of a cylindrical grain boundary with geometric center O . A point P on the grain boundary can be written in polar coordinates as $(R(\alpha), \alpha)$, where $R(\alpha)$ is the radius and α is the polar angle. The normal and tangent directions on the grain boundary are denoted by \mathbf{n} and \mathbf{T} , respectively.

We assume that the cross-section curve of the grain boundary Γ is in the xy plane and the rotation axis is in z direction, and the geometric center (mass center) of the cross-section of the inner grain is the origin O of the xy plane, see Fig. 1. Each point P on the grain boundary can be written in the polar coordinates as (R, α) , where R is the radius and α is the polar angle. We parameterize the two dimensional grain boundary Γ by α , and all the functions defined on Γ , such as R , are functions of the parameter α . In particular, a point on the grain boundary Γ has the coordinate $\mathbf{R}(\alpha) = (x(\alpha), y(\alpha)) = (R(\alpha) \cos \alpha, R(\alpha) \sin \alpha)$. The derivative of a function g defined on the grain boundary with respect to α is denoted by g' , i.e., $g' = dg/d\alpha$. The grain boundary tangent direction \mathbf{T} , the grain boundary normal direction \mathbf{n} , and the curvature of the grain boundary κ at a point $(x(\alpha), y(\alpha))$ on the grain boundary can be calculated as

$$\mathbf{T} = \frac{1}{\sqrt{x'(\alpha)^2 + y'(\alpha)^2}} (x'(\alpha), y'(\alpha)), \quad (1)$$

$$\mathbf{n} = \frac{1}{\sqrt{x'(\alpha)^2 + y'(\alpha)^2}} (-y'(\alpha), x'(\alpha)), \quad (2)$$

$$\kappa = \frac{R(\alpha)^2 + 2R'(\alpha)^2 - R''(\alpha)R(\alpha)}{[R(\alpha)^2 + R'(\alpha)^2]^{3/2}}. \quad (3)$$

The normal direction of the grain boundary \mathbf{n} in Eq. (2) is defined such that $\mathbf{T} \times \mathbf{n} = \mathbf{k}$, where \mathbf{k} is the unit vector in the $+z$ direction. We also have the relations $\frac{d}{d\alpha} = \frac{ds}{d\alpha} \frac{d}{ds}$, where s is the arclength parameter of the grain boundary Γ , and

$$\frac{ds}{d\alpha} = \sqrt{x'(\alpha)^2 + y'(\alpha)^2} = \sqrt{R(\alpha)^2 + R'(\alpha)^2}. \quad (4)$$

Assume that on the grain boundary, there are J dislocation arrays corresponding to J different Burgers vectors $\mathbf{b}^{(j)} = (b_1^{(j)}, b_2^{(j)}, b_3^{(j)})$ with length $b^{(j)} = \|\mathbf{b}^{(j)}\|$, $j = 1, 2, \dots, J$, respectively. All the dislocations are parallel to the z axis, i.e., they are points in the xy plane.

Our continuum model is based on the continuum framework proposed in Zhu and Xiang (2014). The dislocation densities on the grain boundaries are described by the dislocation density potential functions. A dislocation density potential function η is a scalar function defined on the grain boundary such that the constituent dislocations of the same Burgers vector are given by the integer-valued contour lines of η : $\eta = i$, where i is an integer. The dislocation structure can be described in terms of the surface gradient of η on the grain boundary, which is $\nabla_s \eta = \frac{d\eta}{ds} \mathbf{T} = \frac{\eta'(\alpha)}{\sqrt{R(\alpha)^2 + R'(\alpha)^2}} \mathbf{T}$. In particular, the local dislocation line direction is $\mathbf{t} = \frac{\nabla_s \eta}{\|\nabla_s \eta\|} \times \mathbf{n}$, and the inter-dislocation distance along the grain boundary is $D = 1/\|\nabla_s \eta\|$. Accordingly, the dislocation density per unit length on the grain boundary is

$$\rho(\alpha) = \nabla_s \eta \cdot \mathbf{T} = \frac{d\eta}{ds} = \frac{\eta'(\alpha)}{\sqrt{R(\alpha)^2 + R'(\alpha)^2}}. \quad (5)$$

Here we allow the dislocation density ρ to be negative to include dislocations with opposite line directions.

In our continuum model, it is more convenient to use the dislocation density per unit polar angle, which is

$$\varrho(\alpha) = \rho(\alpha) \frac{ds}{d\alpha} = \rho(\alpha) \sqrt{R(\alpha)^2 + R'(\alpha)^2} = \eta'(\alpha). \quad (6)$$

Here we have used Eqs. (4) and (5). The surface gradient $\nabla_s \eta$ can be expressed in terms of ϱ as

$$\nabla_s \eta = \rho(\alpha) \mathbf{T} = \frac{\varrho(\alpha)}{\sqrt{R(\alpha)^2 + R'(\alpha)^2}} \mathbf{T}. \quad (7)$$

The dislocation line direction defined by $\mathbf{t} = \frac{\nabla_s \eta}{\|\nabla_s \eta\|} \times \mathbf{n}$ becomes

$$\mathbf{t} = \frac{\varrho}{|\varrho|} \mathbf{T} \times \mathbf{n}. \quad (8)$$

When there are J dislocation arrays on the grain boundary, these constituent dislocations are represented by $\eta^{(j)}, j = 1, 2, \dots, J$, corresponding to J different Burgers vectors $\mathbf{b}^{(j)}, j = 1, 2, \dots, J$, respectively.

In the continuum framework presented in Zhu and Xiang (2014), the total energy associated with grain boundaries can be written as

$$E = E_{\text{long}} + E_{\text{local}} + E_{\text{other}}, \quad (9)$$

where E_{long} is the energy due to the long-range elastic interaction between the constituent dislocations of the grain boundaries, E_{local} is the line energy of the constituent dislocations corresponding the commonly used grain boundary energy in the literature (Sutton and Bal-luffi, 1995; Read and Shockley, 1950) and is a generalization of the classical Read-Shockley energy formula (Read and Shockley, 1950), and E_{other} includes the energy due to the interactions between the dislocation arrays and other stress fields such as the applied stress.

The variations of this total energy with respect to the change of the grain boundary and the change of dislocation structure on the grain boundary are

$$\frac{\delta E}{\delta r} = - \sum_{j=1}^J \|\nabla_s \eta^{(j)}\| \mathbf{f}_{\text{total}}^{(j)} \cdot \mathbf{n}, \quad \text{when } \delta \mathbf{r} = \mathbf{n} \delta r, \quad (10)$$

$$\frac{\delta E}{\delta \eta^{(j)}} = \mathbf{f}_{\text{total}}^{(j)} \cdot \frac{\nabla_s \eta^{(j)}}{\|\nabla_s \eta^{(j)}\|}, \quad j = 1, 2, \dots, J, \quad (11)$$

respectively, where

$$\mathbf{f}_{\text{total}}^{(j)} = \mathbf{f}_{\text{long}}^{(j)} + \mathbf{f}_{\text{local}}^{(j)} + \mathbf{f}_{\text{other}}^{(j)}. \quad (12)$$

Here $\mathbf{f}_{\text{total}}^{(j)}$ is the total force on the j -th dislocation array, including the force due to the long-range elastic dislocation interaction $\mathbf{f}_{\text{long}}^{(j)}$, the force due to the local interaction between

dislocations $\mathbf{f}_{\text{local}}^{(j)}$, and the force due to other stress fields (such as the applied stress field) $\mathbf{f}_{\text{other}}^{(j)}$, for $j = 1, 2, \dots, J$. These forces are consistent with the Peach-Koehler force on a dislocation in the discrete dislocation dynamics model.

Following the discrete dislocation dynamics model (Xiang et al., 2003; Zhu and Xiang, 2010, 2014), the continuum dynamics of these dislocation arrays along the grain boundary is given by

$$\frac{d\eta^{(j)}}{dt} + \mathbf{v}^{(j)} \cdot \nabla_s \eta^{(j)} = 0, \quad j = 1, 2, \dots, J, \quad (13)$$

where the dislocation velocity $\mathbf{v}^{(j)} = \mathbf{M}_{\text{PK}}^{(j)} \cdot \mathbf{f}_{\text{total}}^{(j)}$, and $\mathbf{M}_{\text{PK}}^{(j)}$ is the mobility associated with the total Peach-Koehler force $\mathbf{f}_{\text{total}}^{(j)}$ of the j -th dislocation array. If in the dynamics process, generation and removal of dislocations are critical, e.g. (Li et al., 1953; Srinivasan and Cahn, 2002; Upmanyu et al., 2006; Wu and Voorhees, 2012; Trautt and Mishin, 2012), using Eq. (11), the dislocation evolution equations are

$$\frac{d\eta^{(j)}}{dt} = -m_j \frac{\delta E}{\delta \eta^{(j)}} = -m_j \left(\mathbf{f}^{(j)} \cdot \frac{\nabla_s \eta^{(j)}}{\|\nabla_s \eta^{(j)}\|} \right), \quad j = 1, 2, \dots, J, \quad (14)$$

where $\mathbf{f}^{(j)}$ is the total force on the j -th dislocation array in Eq. (12) or some of its contributions on the right-hand side, m_j is some positive constant. The choice of Eqs. (13) and/or (14) depends on the physics of the dynamics process. The motion of the grain boundary in general is, following Eq. (10),

$$v_n = -m_n \frac{\delta E}{\delta r} = m_n \sum_{j=1}^J \|\nabla_s \eta^{(j)}\| \mathbf{f}_{\text{total}}^{(j)} \cdot \mathbf{n}, \quad (15)$$

where m_n is the mobility.

This continuum framework is general and applies to any dislocation arrays. Based on this framework, we will develop a two dimensional continuum model for the dynamics of grain boundaries including the motion and tangential translation of the grain boundaries and grain rotation that is consistent with the discrete dislocation dynamics model and atomistic simulations, see the next section. In the two dimensional problems, this new dislocation representation method based on dislocation density potential functions η 's and

the classical method using the scalar dislocation densities are equivalent, see Eqs. (6) and (7). Continuum dynamics model for grain boundaries in three dimensions is being developed and will be presented elsewhere, in which it is more convenient to use dislocation density potential functions for the structure of the constituent dislocations.

3. The continuum model for grain boundary motion

In this section, we present our continuum model for grain boundary motion based on densities of the constituent dislocations. The grain boundary motion is coupled with the evolution of the constituent dislocations on the grain boundary, under both the long-range and local interactions of dislocations. The misorientation angle changes due to the coupling and sliding motions and the shape change of the grain boundary are naturally accommodated by the motion and reaction of the constituent dislocations. A critical idea in the continuum model is that when obtaining the driving force for the grain boundary motion, the variation of the total energy is calculated based on the conservation of the constituent dislocations (Zhu and Xiang, 2014), instead of the fixed grain boundary energy density as did in the literature. An example of such variational derivation is presented in the Appendix for the two dimensional problem in terms of the contribution of the (local) grain boundary energy.

We consider the dynamics of a closed curved grain boundary Γ with radius function $R(\alpha)$ and J dislocation arrays on Γ with Burgers vector $\mathbf{b}^{(j)}$, $j = 1, 2, \dots, J$, as described in the previous section. The motion of the grain boundary and the evolution of the dislocation structure on it are described by

$$v_n = M_d \sum_{j=1}^J \frac{\varrho^{(j)}}{\sum_{k=1}^J \varrho^{(k)}} \left(\mathbf{f}_{\text{long}}^{(j)} + \mathbf{f}_{\text{local}}^{(j)} + \mathbf{f}_{\text{app}}^{(j)} \right) \cdot \mathbf{n} + M_b p, \quad (16)$$

$$\frac{d\varrho^{(j)}}{dt} = -M_d \left(\frac{\varrho^{(j)}}{\sqrt{R^2 + R'^2}} \mathbf{f}_{\text{long}}^{(j)} \cdot \mathbf{T} \right)' - M_t \frac{\partial \gamma}{\partial \varrho^{(j)}} - M_a \left(\frac{\varrho^{(j)}}{|\varrho^{(j)}|} \mathbf{f}_{\text{app}}^{(j)} \cdot \mathbf{T} \right)', \quad (17)$$

$$j = 1, 2, \dots, J.$$

Eq. (16) gives the normal velocity of the grain boundary v_n , where $\mathbf{f}_{\text{long}}^{(j)}$, $\mathbf{f}_{\text{local}}^{(j)}$ and $\mathbf{f}_{\text{app}}^{(j)}$ are the forces on a dislocation with Burgers vector $\mathbf{b}^{(j)}$ due to the long-range elastic interaction

between dislocations, the local interaction between dislocations, and the applied stress field, respectively, and M_d is the mobility of the dislocations. The velocity of a point on the grain boundary is the weighted average of the velocities of dislocations on the grain boundary with different Burgers vectors. This modification has been made from the variational normal velocity formula in Eq. (15) so that the velocity of the grain boundary is consistent with the dynamics of its constituent dislocations (Cahn and Taylor, 2004). Here following the available phase field crystal simulations (Wu and Voorhees, 2012; McReynolds et al., 2016; Yamanaka et al., 2017), we assume that the temperature is high and the dislocation climb mobility is comparable with the glide mobility. Influences of the dislocation glide and climb mobilities on the grain boundary motion will be further explored in the future work. Another driving force for the grain boundary motion is the difference between the bulk energy densities of the two grains denoted by p (Cahn and Taylor, 2004; Trautt and Mishin, 2012), and M_b is the grain boundary mobility associated with this driving force. In the simulations of a finite grain embedded in another one, instead of using the grain boundary normal velocity v_n in Eq. (16) directly, it is more convenient to use the inward radial velocity

$$\frac{dR}{dt} = -v_n \cos \lambda = -\frac{R}{\sqrt{R^2 + R'^2}} v_n, \quad (18)$$

where λ is the angle between the normal direction of the grain boundary and its inward radial direction (see Fig. 1).

Eq. (17) describes the evolution of the dislocation structure on the grain boundary. (Recall that $g' = dg/d\alpha$ for a function $g(\alpha)$.) These equations are based on the dislocation motion along the grain boundary, driven by the forces due to the long-range elastic interaction between dislocations, the local interaction between dislocations, and the applied stress field. The first term in Eq. (17) is the motion of dislocations along the grain boundary following conservation law in Eq. (13) driven by the long-range elastic force. The importance of this term is to maintain the dislocation structure and the condition of cancellation of the far-field stress fields for the grain boundary (or the Frank's formula (Frank, 1950; Bilby, 1955)) in a way that is consistent with the discrete dislocation dynamics. The quantity γ in the second term in Eq. (17) is the grain boundary energy density (when the long-range

elastic interaction vanishes), which comes from the local dislocation interaction. The third term in Eq. (17) is due to the effect of the applied stress. Since the equilibrium dislocation structure on a grain boundary is stable except for the change of the misorientation angle (i.e. sliding along a fixed grain boundary) (Xiang and Yan, 2017), the major influences of the local energy and the applied stress are to change the dislocation structure by reactions (Li et al., 1953; Srinivasan and Cahn, 2002; Upmanyu et al., 2006; Wu and Voorhees, 2012; Trautt and Mishin, 2012), leading to grain boundary sliding. In these processes, the dislocations on the grain boundary are not conserved and the last two terms in Eq. (17) account for such changes of dislocation structure due to these two driving forces (see also Eq. (14)), in which M_t and M_a are the mobilities associated with the driving forces of the local energy and the applied stress, respectively.

In these evolution equations, the continuum long-range force on a dislocation of the j -th dislocation arrays located at the point (x, y) is

$$\mathbf{f}_{\text{long}}^{(j)}(x, y) = \sum_{k=1}^J \int_{\Gamma} \tilde{\mathbf{f}}^{(j,k)}(x, y; x_1, y_1) ds, \quad (19)$$

where ds is the line element of the integral along the grain boundary Γ , the point (x_1, y_1) varies along Γ in the integral, and $\int_{\Gamma} \tilde{\mathbf{f}}^{(j,k)}(x, y; x_1, y_1) ds$ is the force acting on a dislocation of the j -th dislocation array at the point (x, y) generated by the k -th dislocation array, with

$$\tilde{\mathbf{f}}^{(j,k)} = (\tilde{f}_1^{(j,k)}, \tilde{f}_2^{(j,k)}), \quad (20)$$

$$\begin{aligned} \tilde{f}_1^{(j,k)}(x, y; x_1, y_1) = & \frac{\mu}{2\pi(1-\nu)} \frac{1}{[(x-x_1)^2 + (y-y_1)^2]^2} \frac{\varrho^{(k)}(x_1, y_1)}{\sqrt{x_1'^2 + y_1'^2}} \frac{\varrho^{(j)}(x, y)}{|\varrho^{(j)}(x, y)|} \\ & \cdot \left\{ [(x-x_1)^3 - (x-x_1)(y-y_1)^2] b_1^{(k)} b_1^{(j)} \right. \\ & + [(x-x_1)^2(y-y_1) - (y-y_1)^3] b_2^{(k)} b_1^{(j)} \\ & + [(x-x_1)^2(y-y_1) - (y-y_1)^3] b_1^{(k)} b_2^{(j)} \\ & \left. + [(x-x_1)^3 + 3(x-x_1)(y-y_1)^2] b_2^{(k)} b_2^{(j)} \right\}, \end{aligned} \quad (21)$$

$$\begin{aligned}
\tilde{f}_2^{(j,k)}(x, y; x_1, y_1) = & \frac{\mu}{2\pi(1-\nu)} \frac{1}{((x-x_1)^2+(y-y_1)^2)^2} \frac{\varrho^{(k)}(x_1, y_1)}{\sqrt{x_1'^2+y_1'^2}} \frac{\varrho^{(j)}(x, y)}{|\varrho^{(j)}(x, y)|} \\
& \cdot \left\{ [3(x-x_1)^2(y-y_1) + (y-y_1)^3]b_1^{(k)}b_1^{(j)} \right. \\
& + [-(x-x_1)^3 + (x-x_1)(y-y_1)^2]b_2^{(k)}b_1^{(j)} \\
& + [-(x-x_1)^3 + (x-x_1)(y-y_1)^2]b_1^{(k)}b_2^{(j)} \\
& \left. + [-(x-x_1)^2(y-y_1) + (y-y_1)^3]b_2^{(k)}b_2^{(j)} \right\}. \quad (22)
\end{aligned}$$

Here μ is the shear modulus and ν is the Poisson ratio. These formulas can be derived from the continuum long-range elastic force on a low angle grain boundary in three dimensions in Ref. (Zhu and Xiang, 2014) (Eqs. (1) and (13) there) based on the discrete dislocation model (Hirth and Lothe, 1982).

The local force on a dislocation of the j -th dislocation arrays in these evolution equations is

$$\mathbf{f}_{\text{local}}^{(j)} \cdot \mathbf{n} = \frac{\mu(b^{(j)})^2}{4\pi(1-\nu)} \kappa, \quad (23)$$

where κ is the curvature of the grain boundary. The energy density of the short-range interaction of all the dislocations on the grain boundary, i.e., the grain boundary energy density when the long-range elastic fields cancel out, is (Zhu and Xiang, 2014; Zhang et al., 2017a)

$$\gamma = \sum_{j=1}^J \frac{\mu(b^{(j)})^2}{4\pi(1-\nu)} \left[1 - \nu \frac{(\mathbf{T} \times \mathbf{n} \cdot \mathbf{b}^{(j)})^2}{(b^{(j)})^2} \right] \frac{|\varrho^{(j)}|}{\sqrt{R^2 + R'^2}} \log \frac{1}{r_g \sqrt{\varrho^{(j)2}/(R^2 + R'^2) + \epsilon}}, \quad (24)$$

where r_g is a dislocation core parameter and ϵ is a numerical cutoff parameter.

The Peach-Koehler force due to the applied stress $\boldsymbol{\sigma}_{\text{app}}$ is $\mathbf{f}_{\text{app}}^{(j)} = (\boldsymbol{\sigma}_{\text{app}} \cdot \mathbf{b}^{(j)}) \times \mathbf{t}^{(j)}$, where $\mathbf{t}^{(j)}$ is the line direction of a dislocation in the j -th dislocation array on the grain boundary. Using Eq. (8), the contribution of the applied stress the grain boundary velocity given in Eq. (16) can be written as

$$\mathbf{f}_{\text{app}}^{(j)} \cdot \mathbf{n} = -\frac{\varrho^{(j)}}{|\varrho^{(j)}|} (\mathbf{b}^{(j)} \cdot \boldsymbol{\sigma}_{\text{app}} \cdot \mathbf{T}), \quad (25)$$

and the contribution of the applied stress to the dislocation structure evolution equation (17) can be written as

$$\left(\frac{\varrho^{(j)}}{|\varrho^{(j)}|} \mathbf{f}_{\text{app}}^{(j)} \cdot \mathbf{T} \right)' = (\mathbf{b}^{(j)} \cdot \boldsymbol{\sigma}_{\text{app}} \cdot \mathbf{n})' = -\kappa\sqrt{R^2 + R'^2} (\mathbf{b}^{(j)} \cdot \boldsymbol{\sigma}_{\text{app}} \cdot \mathbf{T}), \quad (26)$$

where the last expression holds for a constant applied stress $\boldsymbol{\sigma}_{\text{app}}$, otherwise the expression in the middle should be used.

Remark: Essentially, it is equivalent to use the dislocation density per unit length $\rho^{(j)}$, $j = 1, 2, \dots, J$, as the variables in the continuum grain boundary dynamics model in Eqs. (16) and (17) based on the relation in Eq. (6). However, the evolution equations of $\rho^{(j)}$'s are no longer as simple as Eq. (17) because the arclength of the grain boundary also evolves as the grain boundary migrates.

4. Misorientation angle and effect of long-range dislocation interaction

In our continuum model, the misorientation angle θ between the two grains can be calculated based on the Frank's formula, which is maintained during the motion of the grain boundary by the long-range elastic interaction between the constituent dislocations of the grain boundary.

4.1. Frank's formula and misorientation angle

With the continuum model in Eqs. (16) and (17) for the motion of the grain boundary and evolution of the dislocation structure on it, the misorientation angle θ between the two grains at any point on the grain boundary can be calculated based on the Frank's formula (Frank, 1950; Bilby, 1955), which is a condition for an equilibrium grain boundary dislocation structure and is equivalent to the cancellation of the long-range elastic fields (Frank, 1950; Bilby, 1955; Zhu and Xiang, 2014). Using the representation of dislocation density potential functions, the Frank's formula is (Zhu and Xiang, 2014)

$$\theta(\mathbf{v} \times \mathbf{a}) - \sum_{j=1}^J \mathbf{b}^{(j)} (\nabla_s \eta^{(j)} \cdot \mathbf{v}) = 0, \quad (27)$$

where \mathbf{a} is the rotation axis and \mathbf{v} is any vector tangent to the grain boundary. In the case of two dimensional tilt boundaries being considered in this paper, the rotation axis \mathbf{a} is in the $+z$ direction, and the Frank's formula can be written as

$$\theta \mathbf{n} + \sum_{j=1}^J \rho^{(j)} \mathbf{b}^{(j)} = 0, \quad (28)$$

or

$$\theta \mathbf{n} + \sum_{j=1}^J \frac{\varrho^{(j)} \mathbf{b}^{(j)}}{\sqrt{R^2 + R'^2}} = 0. \quad (29)$$

An equivalent form is

$$\left(\theta \sqrt{R^2 + R'^2} \right) \mathbf{n} + \sum_{j=1}^J \varrho^{(j)} \mathbf{b}^{(j)} = 0. \quad (30)$$

Using the Frank's formula in Eq. (28) or (29), the misorientation angle θ at each point on the grain boundary can be calculated by

$$\theta = - \sum_{j=1}^J \rho^{(j)} (\mathbf{b}^{(j)} \cdot \mathbf{n}) = - \sum_{j=1}^J \frac{\varrho^{(j)} (\mathbf{b}^{(j)} \cdot \mathbf{n})}{\sqrt{R^2 + R'^2}}. \quad (31)$$

Note that an alternative formula to calculate the misorientation angle is $\theta = \|\sum_{j=1}^J \rho^{(j)} \mathbf{b}^{(j)}\| = \|\sum_{j=1}^J \frac{\varrho^{(j)} \mathbf{b}^{(j)}}{\sqrt{R^2 + R'^2}}\|$. Integrating Eq. (31) over the grain boundary, we have

$$\theta = - \frac{1}{L} \int_0^{2\pi} \sum_{j=1}^J \varrho^{(j)} (\mathbf{b}^{(j)} \cdot \mathbf{n}) d\alpha, \quad (32)$$

where L is the circumference of the grain boundary. This formula can be used to evaluate θ during the evolution of the grain boundary in which the shape of the grain boundary and the dislocation densities on it change. In this case, the pointwise formula in Eq. (31) may not give a perfectly constant value over the grain boundary.

4.2. Frank's formula maintained by the long-range dislocation interaction

It has been shown that the Frank's formula is equivalent to the cancellation of the long-range elastic fields generated by the constituent dislocations of the grain boundary

(Frank, 1950; Bilby, 1955; Zhu and Xiang, 2014). In the continuum model in Eqs. (16) and (17), the Frank's formula is maintained by the long-range dislocation interaction. This is because the long-range dislocation interaction is much stronger than the local dislocation interaction (grain boundary energy) except for very small size grain (comparable with the inter-dislocation distance on the grain boundary) (Zhu and Xiang, 2014). As a result, approximately during the motion of the grain boundary, the long-range dislocation interaction vanishes and the Frank's formula holds except when the grain size is very small.

A proof of the equivalence of the Frank's formula and cancellation of the long-range elastic fields generated by the constituent dislocations for a curved grain boundary can be found in Zhu and Xiang (2014). Here we present an alternative calculation in two dimensions to show their equivalence. In fact, the long-range stress field generated by the constituent dislocations of the grain boundary Γ , in the infinite two dimensional space, can be written as

$$\boldsymbol{\sigma}_i(x, y) = \sum_{j=1}^J \int_{\Gamma} \left(\mathbf{G}_1(x, y; x_1, y_1) b_1^{(j)} \rho^{(j)}(x_1, y_1) + \mathbf{G}_2(x, y; x_1, y_1) b_2^{(j)} \rho^{(j)}(x_1, y_1) \right) ds, \quad (33)$$

where the point (x_1, y_1) varies along the grain boundary in the integrals, ds is the line element of the integrals, and

$$\mathbf{G}_1(x, y; x_1, y_1) = \frac{\mu}{2\pi(1-\nu)} \begin{pmatrix} -\frac{(y-y_1)[3(x-x_1)^2+(y-y_1)^2]}{[(x-x_1)^2+(y-y_1)^2]^2} & \frac{(x-x_1)[(x-x_1)^2-(y-y_1)^2]}{[(x-x_1)^2+(y-y_1)^2]^2} \\ \frac{(x-x_1)[(x-x_1)^2-(y-y_1)^2]}{[(x-x_1)^2+(y-y_1)^2]^2} & \frac{(y-y_1)[(x-x_1)^2-(y-y_1)^2]}{[(x-x_1)^2+(y-y_1)^2]^2} \end{pmatrix}, \quad (34)$$

$$\mathbf{G}_2(x, y; x_1, y_1) = \frac{\mu}{2\pi(1-\nu)} \begin{pmatrix} \frac{(x-x_1)[(x-x_1)^2-(y-y_1)^2]}{[(x-x_1)^2+(y-y_1)^2]^2} & \frac{(y-y_1)[(x-x_1)^2-(y-y_1)^2]}{[(x-x_1)^2+(y-y_1)^2]^2} \\ \frac{(y-y_1)[(x-x_1)^2-(y-y_1)^2]}{[(x-x_1)^2+(y-y_1)^2]^2} & \frac{(x-x_1)[(x-x_1)^2+3(y-y_1)^2]}{[(x-x_1)^2+(y-y_1)^2]^2} \end{pmatrix}. \quad (35)$$

Using divergence theorem and the fact that $\frac{\partial}{\partial x_1} \mathbf{G}_1 + \frac{\partial}{\partial y_1} \mathbf{G}_2 = \mathbf{0}$, we have

$$\int_{\Gamma} (\mathbf{G}_1 \theta n_1 + \mathbf{G}_2 \theta n_2) ds = \theta \int_{\Omega} \left(\frac{\partial \mathbf{G}_1}{\partial x_1} + \frac{\partial \mathbf{G}_2}{\partial y_1} \right) dx_1 dy_1 = \mathbf{0}, \quad (36)$$

where $\mathbf{n} = (n_1, n_2)$ is recalled to be the unit normal vector of the grain boundary and Ω is the inner grain. Using Eqs. (33) and (36), the stress field due to the long-range dislocation

interaction can be written as

$$\begin{aligned}\boldsymbol{\sigma}_i(x, y) = & \sum_{j=1}^J \int_{\Gamma} \left[\mathbf{G}_1(x, y; x_1, y_1) \left(b_1^{(j)} \rho^{(j)}(x_1, y_1) - \theta n_1(x_1, y_1) \right) \right. \\ & \left. + \mathbf{G}_2(x, y; x_1, y_1) \left(b_2^{(j)} \rho^{(j)}(x_1, y_1) - \theta n_2(x_1, y_1) \right) \right] ds.\end{aligned}\quad (37)$$

Therefore, the long-range stress field $\boldsymbol{\sigma}_i$, and accordingly the long-range elastic interaction energy of the constituent dislocations, vanish when the Frank's formula in Eq. (28) holds.

5. Grain rotation and coupling and sliding motions

In this section, we present formulas for the rate of change of the misorientation angle $\frac{d\theta}{dt}$ (grain rotation) and the tangential velocities of the coupling and sliding motions of the grain boundary. Derivation of these formulas are based on the Frank's formula, which is maintained by the long-range dislocation interaction in our continuum model in Eqs. (16) and (17).

5.1. Grain rotation

Using the Frank's formula in Eq. (29), it can be calculated that the rate of change of the misorientation angle θ is

$$\frac{d\theta}{dt} = -\frac{\theta}{R} \frac{dR}{dt} + \frac{1}{R} \sum_{j=1}^J \left(\mathbf{b}^{(j)} \cdot \hat{\mathbf{R}} \right) \frac{d\rho^{(j)}}{dt}, \quad (38)$$

where $\hat{\mathbf{R}} = \mathbf{R}/R$ is the outward radial direction of the grain boundary.

Recall that the coupling tangential motion of the grain boundary is associated with conservation of dislocations (Srinivasan and Cahn, 2002; Cahn and Taylor, 2004). From the evolution of dislocation densities in our continuum model in Eq. (17), this means that the mobilities M_t and M_a due to the grain boundary local energy and the applied stress, respectively, are zero, because dislocations are not conserved under these motions. Further with the assumption of Frank's formula, the first term in Eq. (17) due to the long-range dislocation interaction also vanishes. This gives $\frac{d\rho^{(j)}}{dt} = 0$ for all j under the pure coupling motion of the grain boundary. Therefore, the first term in Eq. (38) is associated with the

coupling motion of the grain boundary. The second term in Eq. (38) is due to the change of dislocation densities. As shown above, when $\frac{d\varrho^{(j)}}{dt} \neq 0$, the constituent dislocations are not conserved, leading to the sliding motion of the grain boundary (Srinivasan and Cahn, 2002; Cahn and Taylor, 2004). Denoting these two contributions in Eq. (38) due to the coupling and sliding motions by $\frac{d\theta^c}{dt}$ and $\frac{d\theta^s}{dt}$, respectively, we have

$$\frac{d\theta}{dt} = \frac{d\theta^c}{dt} + \frac{d\theta^s}{dt}, \quad (39)$$

$$\frac{d\theta^c}{dt} = -\frac{\theta}{R} \frac{dR}{dt}, \quad \frac{d\theta^s}{dt} = \frac{1}{R} \sum_{j=1}^J \left(\mathbf{b}^{(j)} \cdot \hat{\mathbf{R}} \right) \frac{d\varrho^{(j)}}{dt}. \quad (40)$$

Note that in some existing continuum models for the motion of grain boundaries and grain rotation (Li, 1962; Kobayashi et al., 2000; Upmanyu et al., 2006; Esedoglu, 2016), evolution of misorientation angle was included to reduce the grain boundary energy density, which are able to capture the grain boundary sliding but not coupling. The grain rotation formula in Eq. (38) in our continuum model incorporates both the coupling and sliding motions and is consistent with the discrete dislocation dynamics model.

The grain rotation formula in Eq. (38) is derived as follows. Taking time derivative in Eq. (29), we have

$$\frac{d\theta}{dt} \mathbf{n} + \theta \frac{d\mathbf{n}}{dt} + \sum_{j=1}^J \varrho^{(j)} \mathbf{b}^{(j)} \frac{d}{dt} \left(\frac{1}{\sqrt{R^2 + R'^2}} \right) + \sum_{j=1}^J \frac{\mathbf{b}^{(j)}}{\sqrt{R^2 + R'^2}} \frac{d\varrho^{(j)}}{dt} = \mathbf{0}. \quad (41)$$

It can be calculated that

$$\frac{d\mathbf{n}}{dt} = \frac{d}{dt} \tan^{-1} \left(\frac{x'}{-y'} \right) \mathbf{T} = \frac{R \frac{dR'}{dt} - R' \frac{dR}{dt}}{R^2 + R'^2} \mathbf{T}. \quad (42)$$

Taking dot product with \mathbf{n} and \mathbf{T} , respectively, in Eq. (41) and using Eq. (42) and the Frank's formula in Eq. (29), we have $\frac{d\theta}{dt} = -\theta \frac{R \frac{dR}{dt} + R' \frac{dR'}{dt}}{R^2 + R'^2} - \sum_{j=1}^J \frac{\mathbf{b}^{(j)} \cdot \mathbf{n}}{\sqrt{R^2 + R'^2}} \frac{d\varrho^{(j)}}{dt}$ and $\theta \frac{R \frac{dR'}{dt} - R' \frac{dR}{dt}}{R^2 + R'^2} = -\sum_{j=1}^J \frac{\mathbf{b}^{(j)} \cdot \mathbf{T}}{\sqrt{R^2 + R'^2}} \frac{d\varrho^{(j)}}{dt}$. The second equation gives $\frac{dR'}{dt} = \frac{R'}{R} \frac{dR}{dt} - \sum_{j=1}^J \frac{\sqrt{R^2 + R'^2}}{\theta R} (\mathbf{b}^{(j)} \cdot \mathbf{T}) \frac{d\varrho^{(j)}}{dt}$, and inserting it into the first equation, we have $\frac{d\theta}{dt} = -\theta \frac{dR}{dt} + \frac{1}{\sqrt{R^2 + R'^2}} \sum_{j=1}^J \left(\frac{R'}{R} \mathbf{b}^{(j)} \cdot \mathbf{T} - \mathbf{b}^{(j)} \cdot \mathbf{n} \right) \frac{d\varrho^{(j)}}{dt}$. This gives Eq. (38) by using the equation that $\frac{R'}{\sqrt{R^2 + R'^2}} \mathbf{T} - \frac{R}{\sqrt{R^2 + R'^2}} \mathbf{n} = \hat{\mathbf{R}}$, which can be obtained using the formulas of \mathbf{T} and \mathbf{n} in Eqs. (1) and (2).

5.2. Coupling and sliding velocities

The tangential velocity of the grain boundary is calculated based on the change of misorientation angle and the fixed center, which is

$$v_{\parallel} = \frac{R}{\cos \lambda} \frac{d\theta}{dt} = \sqrt{R^2 + R'^2} \frac{d\theta}{dt}, \quad (43)$$

where λ is recalled to be the angle between the normal direction of the grain boundary and its inward radial direction, and $\cos \lambda = R/\sqrt{R^2 + R'^2}$, see Fig. 1. By Eqs. (43), (39), (40) and (18), we have

$$v_{\parallel} = v_{\parallel}^c + v_{\parallel}^s, \quad (44)$$

$$v_{\parallel}^c = \sqrt{R^2 + R'^2} \frac{d\theta^c}{dt} = -\frac{\theta \sqrt{R^2 + R'^2}}{R} \frac{dR}{dt} = \theta v_n, \quad (45)$$

$$v_{\parallel}^s = \sqrt{R^2 + R'^2} \frac{d\theta^s}{dt} = \frac{\sqrt{R^2 + R'^2}}{R} \sum_{j=1}^J \left(\mathbf{b}^{(j)} \cdot \hat{\mathbf{R}} \right) \frac{d\varrho^{(j)}}{dt}, \quad (46)$$

where v_{\parallel}^c and v_{\parallel}^s are the tangential velocities of the grain boundary due to the coupling and sliding motions, respectively.

By Eqs. (46) and (17) and the Frank's formula (which means that the long-range dislocation interaction vanishes), we write the sliding velocity v_{\parallel}^s as

$$v_{\parallel}^s = v_{\parallel}^{s,1} + v_{\parallel}^{s,2}, \quad (47)$$

$$v_{\parallel}^{s,1} = -M_t \frac{\sqrt{R^2 + R'^2}}{R} \sum_{j=1}^J \left(\mathbf{b}^{(j)} \cdot \hat{\mathbf{R}} \right) \frac{\partial \gamma}{\partial \varrho^{(j)}}, \quad (48)$$

$$v_{\parallel}^{s,2} = M_a \frac{\kappa(R^2 + R'^2)}{R} \sum_{j=1}^J \left(\mathbf{b}^{(j)} \cdot \hat{\mathbf{R}} \right) (\mathbf{b}^{(j)} \cdot \boldsymbol{\sigma}_{\text{app}} \cdot \mathbf{T}). \quad (49)$$

Here the sliding velocities $v_{\parallel}^{s,1}$ and $v_{\parallel}^{s,2}$ come from variation of the grain boundary local energy and the applied stress, respectively.

When the grain boundary is circular, $R(\alpha)$ is constant, $R'(\alpha) = 0$, $\kappa = 1/R$, and $\mathbf{n} = -\hat{\mathbf{R}}$. At a point on the circular grain boundary where all the dislocations have the same Burgers vector \mathbf{b} that is in the direction $\hat{\mathbf{R}}$, i.e., $b = \mathbf{b} \cdot \hat{\mathbf{R}}$, we have $v_{\parallel}^{s,1} = -M_t b \frac{\partial \gamma}{\partial \varrho}$ and $v_{\parallel}^{s,2} = M_a b^2 \sigma_{\text{rt}}$

, and accordingly,

$$v_{\parallel} = \theta v_n - M_t b \frac{\partial \gamma}{\partial \varrho} + M_a b^2 \sigma_{rt}, \quad (50)$$

where $\sigma_{rt} = \hat{\mathbf{R}} \cdot \boldsymbol{\sigma}_{app} \cdot \mathbf{T}$ is the shear component of the applied stress along the grain boundary. Note that at an arbitrary point on the circular grain boundary, dislocation densities of multiple Burgers vectors are in general nonzero, and the full formula in Eqs. (47)–(49) should be used instead of the simple formula in Eq. (50). As a result, the circular grain boundary may not remain circular during its evolution except for some special cases, e.g., without sliding ($\frac{d\varrho^{(j)}}{dt} = 0$ for all j), see the simulations in the next section.

For this special case of circular grain boundary with single Burgers vector, the tangential velocity of the grain boundary given previously by the Cahn-Taylor model (Cahn and Taylor, 2004; Trautt and Mishin, 2012) is

$$v_{\parallel} = \beta v_n + M_{\parallel} \left(\sigma - \frac{\gamma'(\theta)}{R} \right), \quad (51)$$

where $\beta = \theta$ is the coupling factor, $\gamma'(\theta) = d\gamma/d\theta$, M_{\parallel} is the grain boundary sliding mobility, and σ is the applied shear stress. Comparing Eqs. (50) and (51), we can see that our formula gives the same coupling term (the first term in Eq. (50)) as that in the Cahn-Taylor model. The last two terms in our formula in Eq. (50) that accounts for the grain boundary sliding are also the same as the corresponding terms in the Cahn-Taylor model in Eq. (51) based on the relations $\theta = b/D = |\varrho|b/R$ and $\partial\gamma/\partial|\varrho| = \gamma'(\theta)b/R$ if we further assume $\varrho > 0$ and $M_{\parallel} = M_t b^2 = M_a b^2$.

Therefore, our continuum model generalizes the Cahn-Taylor model (Cahn and Taylor, 2004) by incorporating detailed formulas of the driving forces for the grain boundary coupling and sliding tangential motions that depend on the constituent dislocations, their Burgers vectors, and the grain boundary shape, as well as the shape change of the grain boundaries. For the special case of a circular grain boundary with a single Burgers vector, our tangential velocity formula reduces to the equation in the Cahn-Taylor model.

5.3. Shape-preserving grain boundary motion under pure coupling

Assume that the Frank's formula holds during the evolution of the grain boundary. Taking time derivative in the Franks formula in Eq. (30) and using Eq. (42), we have

$$\frac{d}{dt} \left(\theta \sqrt{R^2 + R'^2} \right) \mathbf{n} + \theta \frac{R \frac{dR'}{dt} - R' \frac{dR}{dt}}{\sqrt{R^2 + R'^2}} \mathbf{T} + \sum_{j=1}^J \frac{d\varrho^{(j)}}{dt} \mathbf{b}^{(j)} = 0. \quad (52)$$

When the tangential motion of the grain boundary is pure coupling, its constituent dislocations are conserved, and we have $\frac{d\varrho^{(j)}}{dt} = 0$, $j = 1, 2, \dots, J$, as shown at the beginning of Sec. 5.1. In this case, since the vectors \mathbf{n} and \mathbf{T} are perpendicular to each other, Eq. (52) gives

$$\frac{d}{dt} \left(\theta \sqrt{R^2 + R'^2} \right) = 0, \quad (53)$$

$$R \frac{dR'}{dt} - R' \frac{dR}{dt} = 0. \quad (54)$$

Integrating Eq. (54) with respect to t , we have $R'(\alpha, t) = C(\alpha)R(\alpha, t)$, where $C(\alpha)$ is some function of α . Integrating this equation with respect to α gives $R(\alpha, t) = A(\alpha)B(t)$, where $A(\alpha)$ and $B(t)$ are some functions. Further using Eq. (53), we have

$$R(\alpha, t) = \frac{\theta(0)}{\theta(t)} R(\alpha, 0). \quad (55)$$

That is, the shape of the grain boundary does not change during the evolution.

In addition to this shape-preserving property, we also have the following identities during the grain boundary motion under conservation of dislocations:

$$\theta(t)R(\alpha, t) = \theta(0)R(\alpha, 0), \quad (56)$$

$$\theta(t)L(t) = \theta(0)L(0), \quad (57)$$

where $L = \int_0^{2\pi} \sqrt{R^2 + R'^2} d\alpha$ is the circumference of the grain boundary. These identities are obtained using Eqs. (55) and (53). We remark that by Eq. (32),

$$L\theta = - \int_0^{2\pi} \sum_{j=1}^J \varrho^{(j)} (\mathbf{b}^{(j)} \cdot \mathbf{n}) d\alpha, \quad (58)$$

which holds generally no matter whether the dislocation densities $\varrho^{(j)}$, $j = 1, 2, \dots, J$ change or not.

Finally, we remark that in the generalized Cahn-Taylor theory based on mass transfer via surface diffusion (Taylor and Cahn, 2007), alternative formulations for grain rotation and grain boundary tangential velocities due to the coupling and sliding as well as the shape-preserving motion for a non-circular grain boundary have been derived. Note that our formulations presented above are based on the dynamics of the constituent dislocations of the grain boundary, instead of the mass transfer mechanism in their formulations.

6. Numerical Simulations

In this section, we perform numerical simulations using our continuum model in Eqs. (16) and (17) to study the motion of grain boundaries and evolution of their dislocation structure in two dimensions. We focus on the grain boundaries in fcc crystals, in which there are $J = 6$ Burgers vectors of the $<110>$ type with the same magnitude b . The cross-section plane of the grain boundaries is the (111) plane, and the directions $[\bar{1}10]$, $[\bar{1}\bar{1}2]$ and $[111]$ are chosen to be the x, y, z directions, respectively. In this coordinate system, the six Burgers vectors are $\mathbf{b}^{(1)} = (1, 0, 0) b$, $\mathbf{b}^{(2)} = \left(\frac{1}{2}, \frac{\sqrt{3}}{2}, 0\right) b$, $\mathbf{b}^{(3)} = \left(\frac{1}{2}, -\frac{\sqrt{3}}{2}, 0\right) b$, $\mathbf{b}^{(4)} = \left(0, \frac{\sqrt{3}}{3}, \frac{\sqrt{6}}{3}\right) b$, $\mathbf{b}^{(5)} = \left(\frac{1}{2}, \frac{\sqrt{3}}{6}, -\frac{\sqrt{6}}{3}\right) b$, and $\mathbf{b}^{(6)} = \left(-\frac{1}{2}, \frac{\sqrt{3}}{6}, -\frac{\sqrt{6}}{3}\right) b$. The rotation axis is fixed as the $[111]$ direction. The misorientation angle of the initial grain boundary in the simulations is 5° . We choose the Poisson's ratio $\nu = 0.347$, which is value of aluminum.

In our simulations, we neglect the applied stress and the bulk energy difference, that is, $\boldsymbol{\sigma}_{\text{app}} = \mathbf{0}$ (accordingly, $\mathbf{f}_{\text{app}}^{(j)} = 0$, $j = 1, 2, \dots, J$) and $p = 0$ in Eqs. (16) and (17). As described in Sec. 3, we use the inward radial velocity $\frac{dR}{dt}$ in Eq. (18) to evolve the grain boundary. The grain boundary motion by Eqs. (16) and (18) is solved using standard forward Euler scheme. The singular integrals in the long-range force $\mathbf{f}_{\text{long}}^{(j)}$ in Eqs. (19)–(22) are calculated using the alternating quadrature rule (Sidi and Israeli, 1988). The evolution

of the dislocation structure in Eq. (17) is solved by the following splitting scheme in time:

$$\frac{\eta_*^{(j)} - \eta^{(j)}(t_n)}{\Delta t} = -M_d \frac{\eta^{(j)'} \sqrt{R^2 + R'^2}}{\sqrt{R^2 + R'^2}} \mathbf{f}_{\text{long}}^{(j)} \cdot \mathbf{T} \Big|_{t=t_n}, \quad (59)$$

$$\frac{\varrho^{(j)}(t_{n+1}) - \varrho_*^{(j)}}{\Delta t} = -M_t \frac{\partial \gamma}{\partial \varrho^{(j)}} \Big|_{t=t_n}, \quad (60)$$

where Δt is the time step. Here recall that $\varrho(\alpha) = \eta'(\alpha)$ or $\eta(\alpha) = \int_0^\alpha \varrho(\alpha_1) d\alpha_1$. The spatial derivative $\eta^{(j)'} \sqrt{R^2 + R'^2}$ in Eq. (59) is calculated using the upwind scheme, and a cutoff parameter is used to set $\eta^{(j)'} = 0$ when the calculated value is very small.

We start from a grain boundary with the equilibrium dislocation structure that satisfies the Frank's formula and has the lowest energy, which can be calculated pointwisely using the method in Zhang et al. (2017a).

We also perform discrete dislocation dynamics simulations to validate our continuum model. The formulation of the interaction between dislocations can be found, e.g., in Hirth and Lothe (1982). In fact, the Peach-Koehler force on a dislocation with Burgers vector $\mathbf{b}^{(i)}$ and line direction $\mathbf{t}^{(i)}$ is $(\boldsymbol{\sigma} \cdot \mathbf{b}^{(i)}) \times \mathbf{t}^{(i)}$, where $\boldsymbol{\sigma}$ is the stress. The stress at a point (x, y) generated by a dislocation located at point (x_1, y_1) with Burgers vector $\mathbf{b}^{(j)} = (b_1^{(j)}, b_2^{(j)})$ and $+z$ line direction is $\boldsymbol{\sigma}^{(j)}(x, y) = \mathbf{G}_1(x, y; x_1, y_1) b_1^{(j)} + \mathbf{G}_2(x, y; x_1, y_1) b_2^{(j)}$, where \mathbf{G}_1 and \mathbf{G}_2 are given in Eqs. (34) and (35).

6.1. Circular grain boundary

We firstly consider the motion of an initially circular grain boundary with radius $R_0 = 140b$. The calculated equilibrium dislocation structure (Zhang et al., 2017a) on this initial grain boundary is shown in Fig 2a, which contains three arrays of dislocations with Burgers vectors $\mathbf{b}^{(1)}$, $\mathbf{b}^{(2)}$, and $\mathbf{b}^{(3)}$, respectively. The distribution of these dislocations are represented by the dislocation density potential functions $\eta^{(1)}$, $\eta^{(2)}$, and $\eta^{(3)}$, respectively, see Fig 2b. Recall that the dislocation density potential functions are defined on the grain boundary such that the constituent dislocations are located at their integer-valued contour lines. Also recall that the dislocation density per unit polar angle $\varrho^{(j)}$ and the dislocation density per unit length $\rho^{(j)}$ can be calculated from $\eta^{(j)}$ using Eqs. (6) and (5). It can be seen that

in this equilibrium dislocation structure, each array of dislocations (with the same Burgers vector) concentrate in two portions of the grain boundary, and on each point on the grain boundary, there are nonzero dislocation densities of two different Burgers vectors (except for some extreme points). In Fig 2b, the locations of dislocations using discrete dislocation model are also shown using the dislocation density potential functions.

6.1.1. Motion under dislocation conservation

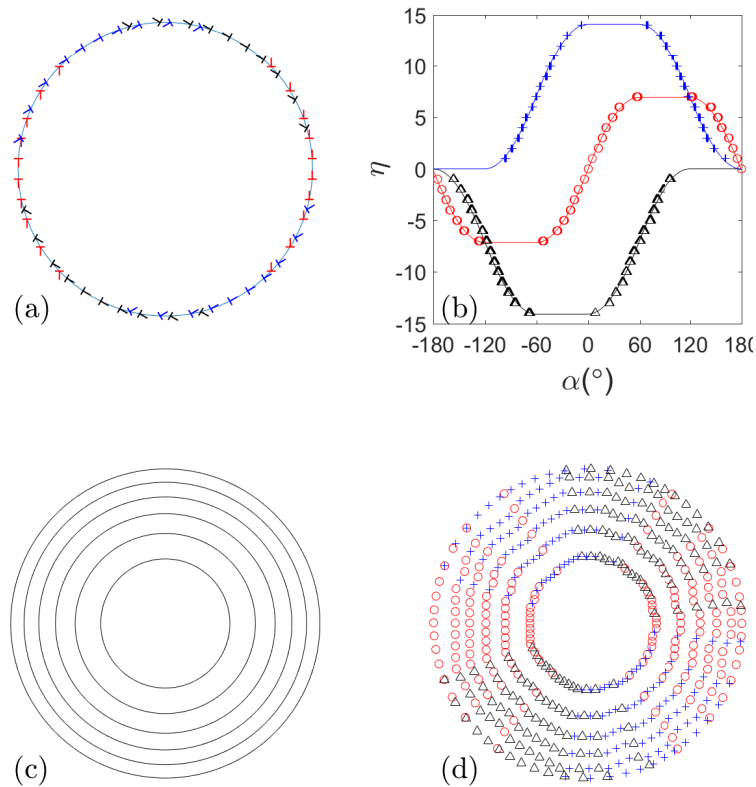


Figure 2: Grain boundary motion under dislocation conservation. The initial grain boundary is circular. (a) Equilibrium dislocation structure on the initial circular grain boundary. There are three arrays of dislocations with Burgers vectors $\mathbf{b}^{(1)}$ (red), $\mathbf{b}^{(2)}$ (black), and $\mathbf{b}^{(3)}$ (blue), respectively. (b) Evolution of dislocation density potential functions of these three arrays of dislocations on the grain boundary (same colors as in (a)). The curves show the results of the continuum model and the dots show the results using the discrete dislocation model. (c) Motion of the grain boundary (shrinkage) by using our continuum model. (d) Motion of the grain boundary by using the discrete dislocation model. In (c) and (d), the grain boundary is plotted at uniform time intervals starting with the outer most one.

In the continuum model in Eqs. (16) and (17), recall that the mobility M_d is associated with the conservative law motion of dislocations and the mobility M_t is associated with dislocation reaction. In the simulations in this subsection, we set $M_t = 0$, i.e., the dislocations move entirely by the conservation law without dislocation reaction. This can happen to low angle grain boundaries whose sizes are not very small, as observed in atomistic (Srinivasan and Cahn, 2002) and phase-field crystal (Wu and Voorhees, 2012) simulations.

Figure 2c and 2d show the evolution of the grain boundary obtained by using our continuum model and the discrete discrete model, respectively, under the same initial configuration and dislocation mobility. In the simulation results of the continuum model shown in Fig 2c, the circular grain boundary shrinks with increasing rate and keeps the circular shape during the shrinkage. This evolution is in excellent agreement with the simulation results using the discrete dislocation model shown in Fig 2d.

The evolutions of the dislocation structure during the shrinking of this grain boundary by using the continuum model and the discrete dislocation model are shown in Fig 2b, based on the dislocation density potential functions $\eta^{(1)}$, $\eta^{(2)}$, and $\eta^{(3)}$ for dislocations with Burgers vectors $\mathbf{b}^{(1)}$, $\mathbf{b}^{(2)}$, and $\mathbf{b}^{(3)}$, respectively, as illustrated at the beginning of this section. We can see from this figure that the dislocation density potential functions using both the continuum model and the discrete model maintain their initial profiles during the evolution, meaning that the dislocation densities per unit polar angle do not change. This means that all the dislocations move in the inward radial direction of the grain boundary using both models, as can also be seen from the results of the discrete model shown in Fig 2d. These simulation results agree with the theoretic prediction of $\frac{d\eta^{(j)}}{dt} = 0$ for all j under the conservation of dislocations shown at the beginning of Sec. 5.1. The Frank's formula always holds and the long-range dislocation interaction vanishes during the motion of this circular grain boundary.

In this simulation, the grain rotates by pure coupling effect as it shrinks. We calculate the misorientation angle θ during the shrinkage of the circular grain boundary by Eq. (31) (where $R' \equiv 0$). Fig. 3a shows the misorientation angle θ and $1/\theta^2$ as functions of the evolution time t . In Fig. 3b, the radius R of the evolving circular grain boundary, as well as the

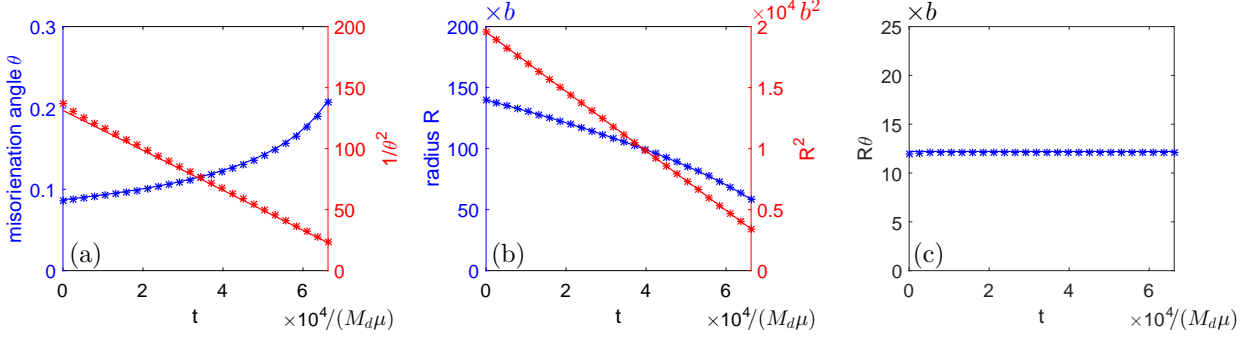


Figure 3: Grain boundary motion under dislocation conservation. The initial grain boundary is circular. (a) The misorientation angle θ as a function of evolution time. (b) The radius R as a function of evolution time. (c) $R\theta$ keeps constant during the evolution. The curves show the results of the continuum model and the dots show the results using the discrete dislocation model.

quantity R^2 are shown in terms of t . It can be seen that the misorientation angle θ increases as the grain boundary shrinks, and the changing rates of both θ and R are increasing. More precisely, the quantities $1/\theta^2$ and R^2 decrease linearly with t . We also examine the relation between the radius R and misorientation θ , and it can be seen that their multiplication $R\theta$ is constant during the evolution as shown in Fig. 3c. This relation agrees with the theoretical prediction by Eq. (56). Moreover, by the grain boundary evolution equation in Eq. (16), for this circular grain boundary, the long-range force \mathbf{f}_{long} vanishes as discussed above, and the evolution equation is reduced to $v_n = \frac{M_d \mu b^2}{4\pi(1-\nu)R}$ and $\frac{dR}{dt} = -v_n$. This implies that $R(t)^2$ is a linear function of t : $R(t)^2 = R(0)^2 - \frac{M_d \mu b^2}{2\pi(1-\nu)}t$. Accordingly, $1/\theta(t)^2$ is also a linear function of t due to the fact that $R(t)\theta(t)$ remains constant. The simulation results discussed above agree with these theoretical predictions. Especially, both the slope of the numerical $R^2(t)$ curve in Fig. 3b and the theoretical formula of the slope $\frac{dR^2}{dt} = -\frac{M_d \mu b^2}{2\pi(1-\nu)}$ give the same value $-0.2437 M_d \mu b^2$.

During the shrinkage of this circular grain boundary, the tangential velocity v_{\parallel} and the normal velocity v_n of the grain boundary should satisfy the coupling relation $v_{\parallel} = v_{\parallel}^c = \theta v_n$ by the Cahn-Taylor theory (Cahn and Taylor, 2004) or our Eq. (45). We examine this relation by our continuum simulation as shown in Fig. 4. The tangential velocity v_{\parallel} and

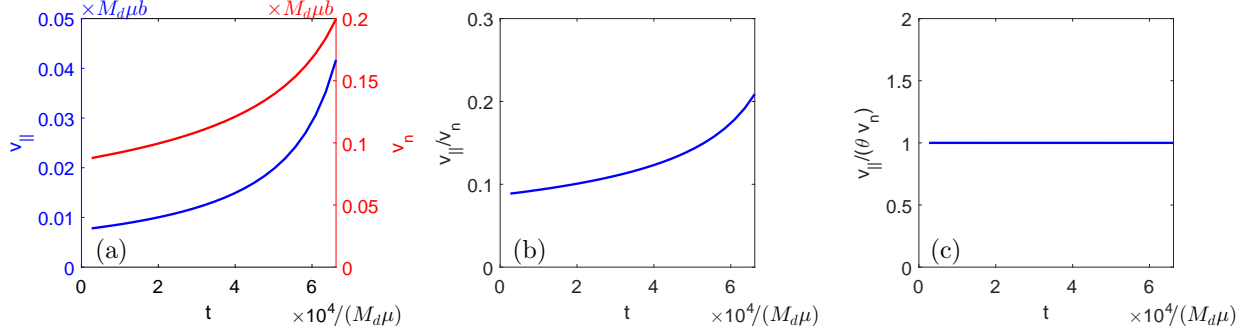


Figure 4: Grain boundary motion under dislocation conservation. The initial grain boundary is circular. (a) The tangential velocity v_{\parallel} and normal velocity v_n of the grain boundary. (b) The ratio v_{\parallel}/v_n . (c) Verification of the coupling relation $v_{\parallel} = \theta v_n$.

the normal velocity v_n during the evolution of the circular grain boundary are plotted in Fig. 4a, where v_{\parallel} is calculated by $v_{\parallel} = R \frac{d\theta}{dt}$ using Eq. (43). The relation of the two velocities obtained from our simulation results are shown in Fig. 4b and Fig. 4c. Excellent agreement can be seen between the numerical and theoretical values for the coupling relation $v_{\parallel} = \theta v_n$.

These simulation results of the continuum model and the discrete dislocation model agree excellently with the available atomistic (Srinivasan and Cahn, 2002) and phase-field crystal (Wu and Voorhees, 2012) simulations, and the Cahn-Taylor theory (Cahn and Taylor, 2004) which is a mechanism without details of the dislocation structure on the grain boundary.

6.1.2. With dislocation reaction

In this subsection, we perform simulations using our continuum model for the case in which dislocation reaction is not negligible during the motion of the grain boundary, i.e., $M_t \neq 0$. The simulation results from the initial, circular grain boundary with $M_t b / M_d = 0.286 \times 10^{-4}$ are shown in Fig. 5a. The initial circular grain boundary gradually changes to hexagonal shape as it shrinks. Evolution of the dislocation density potential functions $\eta^{(j)}$, $j = 1, 2, 3$, is shown in Fig. 5c. The amplitude of each $\eta^{(j)}$ is decreasing, meaning that the dislocations react and the number of dislocations of each Burgers vector is reduced. For the purpose of comparison, in the discrete dislocation dynamics simulation, we manually remove

two pairs of dislocations in each of the three arrays of dislocations with different Burgers vectors in the initial dislocation structure of the circular grain boundary, and the simulation results are shown in Fig. 5b. The grain boundary profile obtained in this discrete dislocation dynamics simulation also shows that the grain boundary evolves towards a hexagonal shape. Excellent qualitative agreement can be seen from the simulation results using these two models. Note that in the simulations using our continuum model, dislocations are removed continuously during the motion of the grain boundary.

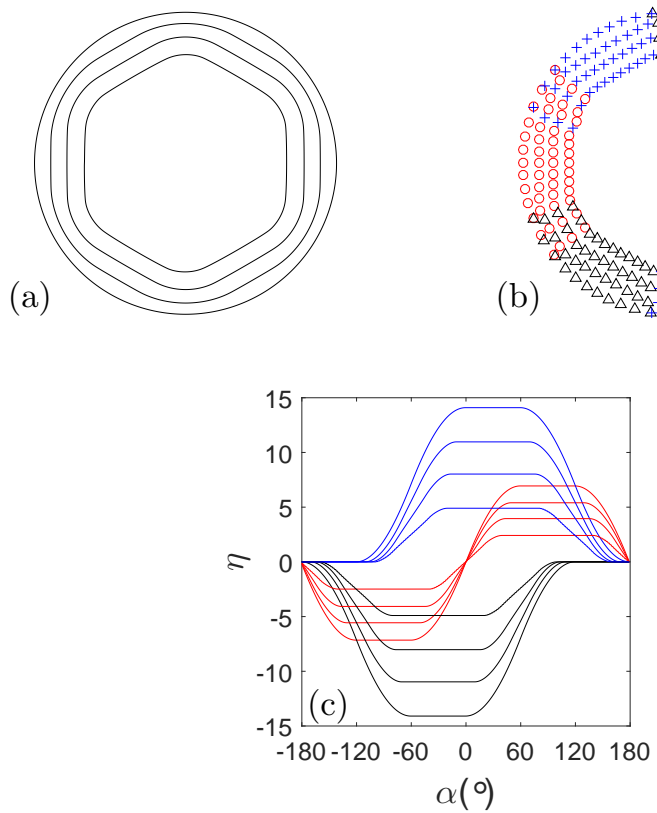


Figure 5: Grain boundary motion with dislocation reaction: $M_t b / M_d = 0.286 \times 10^{-4}$. The initial grain boundary is circular. (a) Grain boundary motion using our continuum model. The grain boundary is plotted at uniform time intervals starting with the outer most one. (b) Grain boundary motion by using discrete dislocation dynamics model, where two pairs of dislocations in each of the three arrays of dislocations with different Burgers vectors are removed in the initial dislocation structure of the circular grain boundary. (c) Evolution of the dislocation density potential functions $\eta^{(1)}$, $\eta^{(2)}$, and $\eta^{(3)}$ of the three arrays of dislocations with Burgers vectors $\mathbf{b}^{(1)}$ (red), $\mathbf{b}^{(2)}$ (black), and $\mathbf{b}^{(3)}$ (blue), respectively.

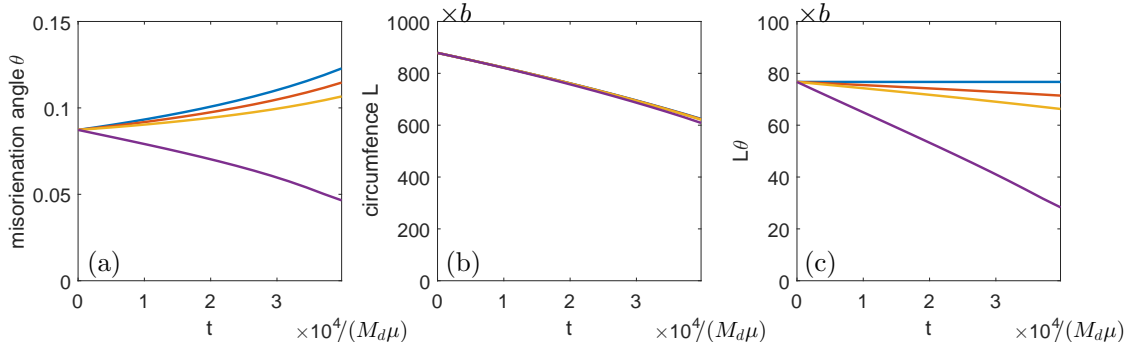


Figure 6: Grain boundary motion with dislocation reaction for different reaction mobility M_t : $M_t b/M_d = 0, 2.86 \times 10^{-5}, 5.762 \times 10^{-5}$, and 2.86×10^{-4} (from the top to the bottom). The initial grain boundary is circular. (a) Evolution of the misorientation angle θ . (b) Evolution of the circumference of the grain boundary L . (c) Evolution of $L\theta$.

Evolution of the misorientation angle θ of this initial circular grain boundary with different values of reaction mobility M_t is shown in Fig. 6a, using the formula in Eq. (32). In this case, the evolution of the misorientation angle θ is controlled by both the coupling effect that depends on the dislocation mobility M_d and the sliding effect that depends mainly on the mobility M_t due to dislocation reaction. The coupling effect increases the misorientation angle θ while the sliding effect decreases θ . This can be understood as follows. At a point on the initial circular grain boundary where all the dislocations have the same Burgers vector \mathbf{b} that is in the outward radial direction $\hat{\mathbf{R}}$, by Eqs. (38), (17), and (24) together with the cancellation of the long-range force in the initial dislocation structure, we have

$$\frac{d\theta}{dt} = \frac{M_d \mu b^2 \theta}{4\pi(1-\nu)R^2} - \frac{M_t \mu b^3}{4\pi(1-\nu)R^2} \log \left(\frac{1}{er_g \sqrt{\rho^2/R^2 + \epsilon}} \right). \quad (61)$$

The first term in this equation is due to the coupling effect and increases the misorientation angle θ , whereas the second term is due to the sliding effect and decreases θ . Note that the above equation is just for qualitative understanding because here we have dislocations with three different Burgers vectors and the grain boundary shape also changes during the evolution. As can be seen from the simulation results in Fig. 6a, when the dislocation reaction mobility M_t increases, meaning the sliding effect due to dislocation reaction is becoming stronger, the increase rate of θ is decreasing during the motion of the grain boundary, and

when the sliding effect is strong enough, the misorientation angle θ is decreasing.

Evolutions of the circumference of the grain boundary L and the product $L\theta$ are shown in Fig. 6b and Fig. 6c. Note that here we consider the circumference for a non-circular grain boundary instead of the radius R for a circular one. Recall that in the case without dislocation reaction discussed previously, $L\theta = 2\pi R\theta$ keeps constant during the evolution of the grain boundary. When sliding effect is not negligible, $L\theta$ is decreasing during the evolution of the grain boundary due to the fact that the sliding effect decreases the misorientation angle, as shown in Fig. 6c, which is also in agreement with Eq. (58). However, the evolution of the circumference of the grain boundary L does not change much for these values of $M_t b/M_d$ compared with the case of $M_t = 0$, see Fig. 6b.

6.2. Elliptic grain boundary

We then consider the motion of a grain boundary with initial shape of ellipse. The long axis of the ellipse is $140b$ and the ratio of the long axis to the short axis is 1.5, see the outer most curve in Fig 7a. As in the circular grain boundary case, the equilibrium dislocation configuration on this elliptic grain boundary also consists of dislocations with Burgers vectors $\mathbf{b}^{(1)}$, $\mathbf{b}^{(2)}$, and $\mathbf{b}^{(3)}$, represented by dislocation density potential functions $\eta^{(1)}$, $\eta^{(2)}$, and $\eta^{(3)}$, respectively, as shown in Fig 7c. The locations of dislocations on this grain boundary using discrete dislocation model are also shown in Fig 7c based on the dislocation density potential functions.

6.2.1. Motion under dislocation conservation

We first consider the motion of this initially elliptical grain boundary under dislocation conservation without dislocation reaction, i.e., $M_t = 0$. In this case, the grain boundary motion is pure coupling and there is no sliding effect. Simulation result using our continuum model is shown in Fig 7a. We can see that the elliptic grain boundary shrinks with increasing rate and its shape does not change during the evolution. We also perform simulation using the discrete dislocation dynamics model to validate our continuum model, and the result is plotted in Fig 7b, which shows that all the dislocations move in the inward radial direction and the shape of the grain boundary is also preserved. As discussed in Secs. 5.3 and 4.2, this

shape-preserving property obtained by using our continuum model and the discrete dislocation model is a result of the Frank's formula that is maintained by the long-range interaction between dislocations, and is in agreement with the prediction of the generalization of the Cahn-Taylor theory to noncircular grains based on mass transfer by surface diffusion (Taylor and Cahn, 2007).

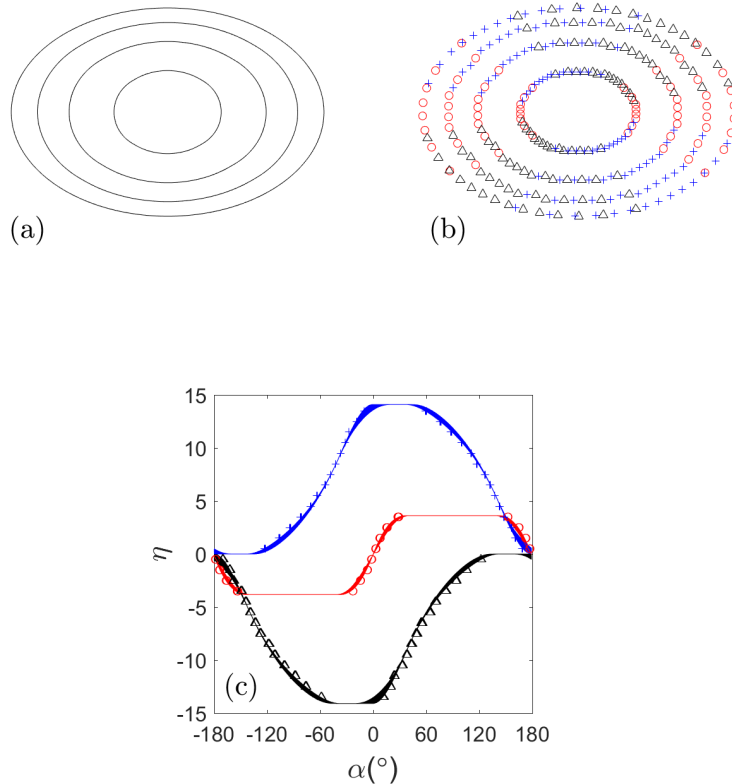


Figure 7: Grain boundary motion under dislocation conservation. The initial grain boundary is an ellipse. (a) Motion of the grain boundary (shrinkage) by using our continuum model. (b) Motion of the grain boundary by using the discrete dislocation model. In (a) and (b), the grain boundary is plotted at uniform time intervals starting with the outer most one. (c) Evolution of dislocation density potential functions $\eta^{(1)}$, $\eta^{(2)}$, and $\eta^{(3)}$, which represent dislocations on the grain boundary with Burgers vectors $\mathbf{b}^{(1)}$ (red), $\mathbf{b}^{(2)}$ (black), and $\mathbf{b}^{(3)}$ (blue), respectively. The curves show the results of the continuum model and the dots show the results using the discrete dislocation model.

Evolutions of the dislocation structure on this grain boundary represented by dislocation density potential functions $\eta^{(1)}$, $\eta^{(2)}$, and $\eta^{(3)}$ are shown in Fig 7c. It can be seen that

these functions do not change as the grain boundary shrinks, by using both the discrete dislocation model and the continuum model up to numerical errors. These simulation results indicate that the dislocation densities per unit polar angle, $\varrho^{(j)} = \eta^{(j)'}$, $j = 1, 2, 3$, do not change during the evolution of the grain boundary. Since this property is a corollary of the Frank's formula as discussed at the beginning of Sec. 5.1, the simulation results using both the discrete and continuum models justify the assumption that the Frank's formula holds during the evolution of the grain boundary, based on which the formulas and properties of the misorientation angle, grain rotation and coupling and sliding motions are derived in Secs. 4 and 5.

We believe the small errors in the numerical results of the continuum model compared with the discrete model seen in Fig 7c are mainly due to the forward Euler type numerical schemes used in our simulations, see the beginning of this section. Note that this paper focus on derivation of the continuum model. Efficient and accurate numerical schemes for this continuum model will be explored in the future work.

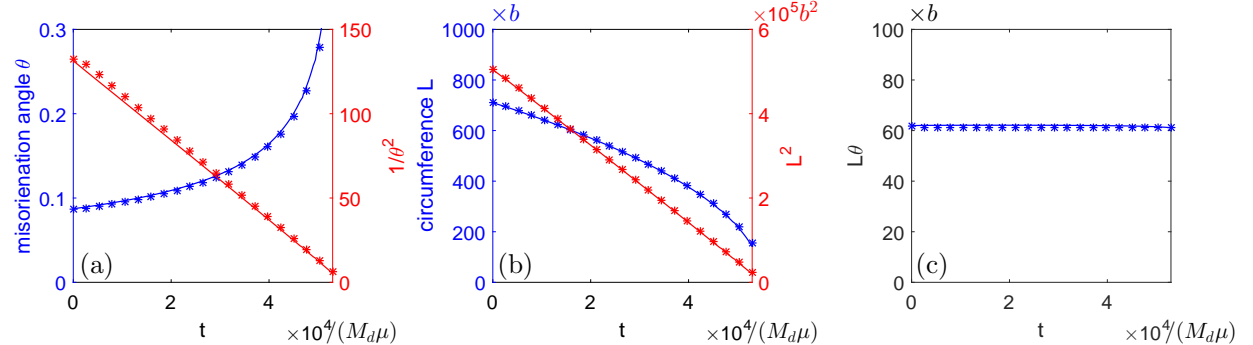


Figure 8: Grain boundary motion under dislocation conservation. The initial grain boundary is an ellipse. (a) The misorientation angle θ as a function of evolution time. (b) The circumference of the grain boundary L as a function of evolution time. (c) $L\theta$ keeps constant during the evolution. The curves show the results of the continuum model and the dots show the results using the discrete dislocation model.

Next, we examine the evolution of the misorientation angle θ , which is calculated by using Eq. (32) during the evolution of the grain boundary. Fig. 8a shows the misorientation angle θ as a function of the evolution time t . It can be seen that as in the simulation of a

circular grain boundary, θ increases during the evolution and $1/\theta^2$ is a linear function of t . Evolution of the circumference of the elliptic grain boundary, L , is shown in Fig. 8b. The simulation results show that L is decreasing and L^2 is a linear function of t , as the behavior of the radius of the circular grain boundary R in the simulations in Sec. 6.1.1. These results are in excellent agreement with the discrete dislocation dynamics simulations. In this case, the quantity $L\theta$ does not change during the evolution, as the quantity $R\theta$ in the simulations of a circular grain in Sec. 6.1.1. This also agrees excellently with the discrete dislocation dynamics simulations as shown in Fig. 8c.

6.2.2. With dislocation reaction

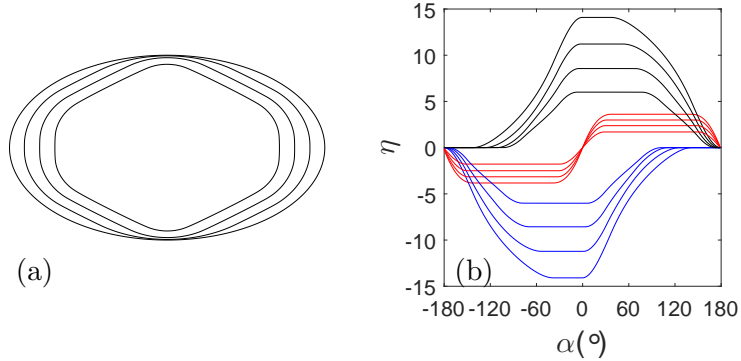


Figure 9: Grain boundary motion with dislocation reaction: $M_t b / M_d = 0.286 \times 10^{-4}$. The initial grain boundary is an ellipse. (a) Grain boundary motion using our continuum model. The grain boundary is plotted at uniform time intervals starting with the outer most one. (b) Evolution of the dislocation density potential functions $\eta^{(1)}$, $\eta^{(2)}$, and $\eta^{(3)}$ of the three arrays of dislocations with Burgers vectors $\mathbf{b}^{(1)}$ (red), $\mathbf{b}^{(2)}$ (black), and $\mathbf{b}^{(3)}$ (blue), respectively.

In this subsection, we perform simulations from the initially elliptical grain boundary for the case in which dislocation reaction is not negligible during the motion of the grain boundary, i.e., $M_t \neq 0$. The simulation results of the circular grain boundary with $M_t b / M_d = 0.286 \times 10^{-4}$ are shown in Fig. 9a. The initial circular grain boundary gradually changes to hexagonal shape as it shrinks, as the simulations from a circular grain boundary with dislocation reaction presented in Sec. 6.1. Evolution of the dislocation density potential functions $\eta^{(j)}$, $j = 1, 2, 3$, is shown in Fig. 9b. Again as the simulations from a circular

grain boundary with dislocation reaction presented in Sec. 6.1, the amplitude of each $\eta^{(j)}$ is decreasing, meaning that the dislocations react and the number of dislocations of each Burgers vector is reduced.

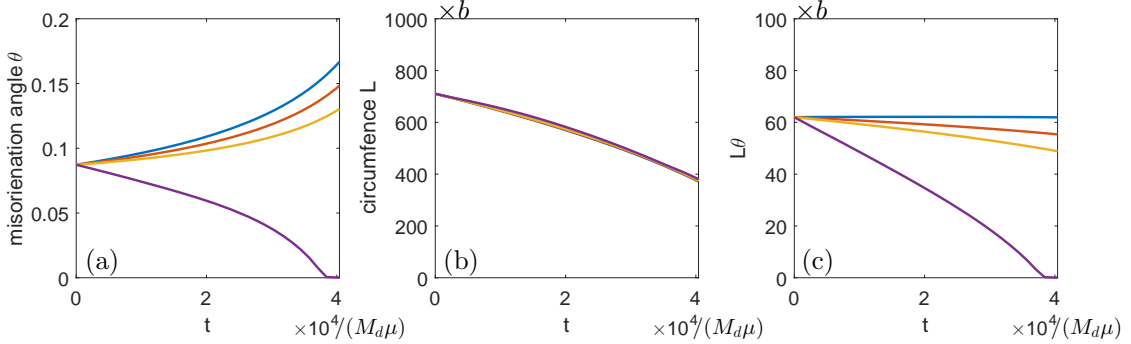


Figure 10: Grain boundary motion with dislocation reaction for different reaction mobility M_t : $M_t b/M_d = 0, 2.86 \times 10^{-5}, 5.762 \times 10^{-5}$, and 2.86×10^{-4} (from the top to the bottom). The shape of the initial grain boundary is an ellipse. (a) Evolution of the misorientation angle θ . (b) Evolution of the circumference of the grain boundary L . (c) Evolution of $L\theta$.

Evolution of the misorientation angle θ from this initial elliptic grain boundary with different values of the reaction mobility M_t is shown in Fig. 10a, compared with the evolution of θ with $M_t = 0$ discussed previously. As discussed in the simulations of circular grain boundaries, the coupling effect that depends on the dislocation mobility M_d increases the misorientation angle θ , while the sliding effect that depends mainly on the mobility M_t due to dislocation reaction decreases θ . When the dislocation reaction mobility M_t increases, meaning the sliding effect due to dislocation reaction is becoming stronger, the increase rate of θ is decreasing during the motion of the grain boundary, and when the sliding effect is strong enough, the misorientation angle θ is decreasing.

Evolutions of the circumference of the grain boundary L and the product $L\theta$ are shown in Fig. 10b and Fig. 10c. Again as in the simulations of a circular grain boundary, the product $L\theta$ keeps constant in the case of $M_t = 0$ due to the pure coupling effect; whereas with dislocation reaction, the sliding effect is no longer negligible, and $L\theta$ is decreasing during the evolution of the grain boundary due to the fact that the sliding effect decreases the misorientation angle, as shown in Fig. 10c. The evolution of the circumference of the

grain boundary L does not change much for these values of M_t compared with the case of $M_t = 0$, see Fig. 10b.

6.3. Pointwise misorientation angle θ

In the simulations presented above, we calculate the misorientation angle θ of the grain boundary based on the formula in Eq. (32), which is an average of the pointwise misorientation angle along the grain boundary given by Eq. (31) based on the Frank's formula. In this subsection, we examine the pointwise misorientation angle formula in Eq. (31) using the simulation results of our continuum model.

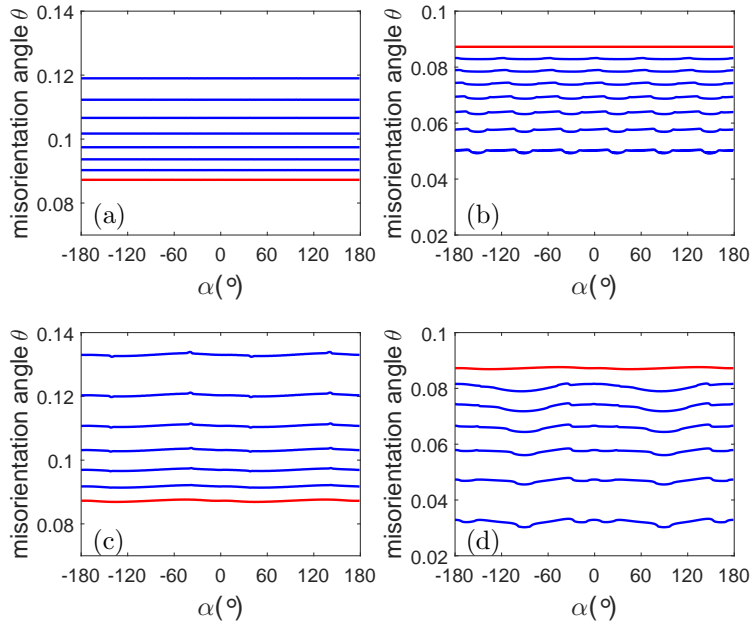


Figure 11: Pointwise misorientation angle θ during the motion of the grain boundary, plotted at uniform time interval. The red line shows the values of θ on the initial grain boundary. (a) The shape of the initial grain boundary is a circle, under dislocation conservation. (b) The shape of the initial grain boundary is a circle, with dislocation reaction. (c) The shape of the initial grain boundary is an ellipse, under dislocation conservation. (d) The shape of the initial grain boundary is an ellipse, with dislocation reaction. In (b) and (d), $M_t b / M_d = 0.286 \times 10^{-4}$.

Fig. 11a shows the pointwise misorientation angle θ for the simulation of the motion of the circular grain boundary under dislocation conservation presented in Sec. 6.1.1. As shown

there, θ increases as the grain boundary evolves due to the pure coupling motion. In this case, θ is constant perfectly throughout the grain boundary during its motion. Fig. 11b shows the calculated pointwise value of θ for the simulation of the motion of the initially circular grain boundary with dislocation reaction presented in Sec. 6.1.2, where the mobility M_t associated with dislocation reaction is relatively large and θ decreases as the grain boundary evolves due to the strong sliding effect. In this case, θ is also a constant approximately throughout the grain boundary during its motion. Note that the grain boundary is no longer circular once it evolves.

The pointwise values of the misorientation angle θ for the motion of an initially elliptical grain boundary under dislocation conservation are shown Fig. 11c. These values are calculated based on the simulation results presented in Sec. 6.2.1, where θ increases as the grain boundary evolves. In this case, θ is also constant throughout the grain boundary during its motion. Fig. 11d shows the calculated pointwise value of θ for the simulation of the motion of the initially elliptical grain boundary with dislocation reaction presented in Sec. 6.2.2, where the mobility M_t is relatively large and θ decreases as the grain boundary evolves with change in its shape. In this case, θ is approximately a constant with a slight undulation over the grain boundary during its motion. The small deviation from a perfect constant of the pointwise misorientation angle θ on the grain boundary in Fig. 11b and d is due to the fact that the long-range elastic interaction between the constituent dislocations of the grain boundary that maintains the Frank's formula is finite, thus is not able to keep the Frank's formula instantly during the evolution.

These numerical results show that the pointwise misorientation angle formula in Eq. (31) indeed holds throughout the grain boundary during its evolution. Since Eq. (31) is derived from the Frank's formula, these simulation results also provide a justification that the Frank's formula holds pointwise during the motion of the grain boundary, which is the basis for the formulas in Eqs. (31) and (32) for the misorientation angle (pointwise and averaged, respectively), Eq. (38) for the grain rotation, and Eqs. (44)–(49) for the tangential velocity of the grain boundary.

7. Conclusions and discussion

In this paper, we have presented a continuum model for the dynamics of low angle grain boundaries in two dimensions incorporating both the motion of grain boundaries and the dislocation structure evolution on the grain boundaries (Eqs. (16) and (17)). The long-range elastic interaction between dislocations is included in the continuum model, which maintains the dislocation structures on the grain boundaries and ensures that they are consistent with the condition of Frank's formula for grain boundaries, i.e., the condition of cancellation of the far-field elastic fields. These evolutions of the grain boundary and its dislocation structure are able to describe both motion and tangential translation of grain boundaries and grain rotation due to both coupling and sliding. Since the continuum model is based upon dislocation structure, it naturally accounts for the grain boundary shape change during the motion and rotation of the grain boundary by motion and reaction of the constituent dislocations without explicit mass transfer. See Eqs. (31) and (32) for the pointwise and averaged misorientation angle formulas, Eq. (38) for the grain rotation formula, and Eqs. (44)–(49) for the tangential velocity formula, derived using this continuum grain boundary dynamics model.

Our continuum grain boundary dynamics model is based upon the continuum framework for grain boundaries in Zhu and Xiang (2014) derived from the discrete dislocation dynamics model, which is the basis for the development of grain boundary models and understanding of simulation and experimental results for grain boundaries (Read and Shockley, 1950; Li et al., 1953; Srinivasan and Cahn, 2002; Cahn and Taylor, 2004; Cahn et al., 2006b,a; Molodov et al., 2007; Gorkaya et al., 2009; Trautt and Mishin, 2012; Wu and Voorhees, 2012; McReynolds et al., 2016; Yamanaka et al., 2017; Lim et al., 2009; Quek et al., 2011; Lim et al., 2012).

Compared with the theory of Cahn-Taylor (Cahn and Taylor, 2004), our continuum model generalizes it by (1) incorporating detailed formulas of the driving forces for the normal and tangential grain boundary velocities that depend on the constituent dislocations, their Burgers vectors, and the grain boundary shape, and (2) incorporating the shape change

of the grain boundaries. Our model is different from their earlier generalized model based on mass transfer via surface diffusion (Taylor and Cahn, 2007). Compared with the existing continuum models for the motion of grain boundaries and grain rotation based on evolution of the misorientation angle (Li, 1962; Kobayashi et al., 2000; Upmanyu et al., 2006; Esedoglu, 2016), our dislocation-structure based continuum model is able to further describe the grain rotation due to the coupling of normal and tangential motions of the grain boundaries, which is missing in these existing models.

Using the derived continuum grain boundary dynamic model, simulations are performed for the dynamics of circular and non-circular two dimensional grain boundaries, and the results are validated by discrete dislocation dynamics simulations. Simulations of both continuum and discrete models show that Frank's formula holds approximately during the evolution of the grain boundary, and is maintained by the long-range elastic interaction of the constituent dislocations. For a finite grain embedded in another one with a low misorientation angle θ , the coupling motion increases θ while the sliding motion reduces θ . Simulations also show that when the grain boundary motion is pure coupling, its shape is preserved (which agrees with prediction of the Cahn-Taylor model based on mass transfer via surface diffusion (Taylor and Cahn, 2007)), and the product $L\theta$ keeps constant, where L is the circumference of the grain boundary. The product $L\theta$ is decreasing when the sliding effect is not negligible during the motion of the grain boundary. In general, a grain boundary is not able to maintain a circular shape during its evolution except for some special cases.

The continuum model for the dynamic of low angle grain boundary presented in this paper can be generalized to polycrystals which contains multiple grains and grain boundary junctions. Generalizations can also be made to grain boundaries in three dimensions. These will be explored in the future work. Finally, we remark that continuum model for the dynamics of high angle grain boundaries has also been developed (Zhang et al., 2017b) based on a disconnection model and atomistic simulations (Thomas et al., 2017).

Appendix A. Variational derivation of the continuum model for grain boundary motion

In the classical theories for the motion of grain boundaries, the driving force is obtained by variation of the grain boundary energy whose density does not evolve as the grain boundary migrates (Herring, 1951; Mullins, 1956; Sutton and Balluffi, 1995). Although in some models, further variations have been taken to reduce the grain boundary energy density (grain boundary sliding) (Li, 1962; Kobayashi et al., 2000; Upmanyu et al., 2006; Esedoglu, 2016), these models are not able to include the grain boundary coupling motion in which the grain boundary energy density may increase (Srinivasan and Cahn, 2002; Cahn and Taylor, 2004).

In the continuum framework for grain boundaries and dislocation arrays proposed in Zhu and Xiang (2014), the driving force for grain boundary or dislocation array motion was obtained by taking variation of the total energy with respect to the change of the grain boundary profile under the conservation of the constituent dislocations. This enables the incorporation of both the coupling and sliding motions of the grain boundary when it evolves. This continuum framework is general: it applies to dislocation structures on grain boundaries in three dimensions and includes both the long-range and short-range interactions of the constituent dislocations.

In this Appendix, we present an example of such variation method for the derivation of the continuum grain boundary motion model in two dimensions, in terms of the contribution of the grain boundary energy due to the local interaction of dislocations which is the commonly used grain boundary energy in the literature. This approach is a generalization of that by Srinivasan and Cahn (2002) and Cahn and Taylor (2004) for two dimensional circular grain boundaries, and is different from the model by Talor-Cahn based on explicit mass transfer along the grain boundaries (Taylor and Cahn, 2007).

Consider a grain boundary Γ as shown in Fig. 1. For the purpose of demonstration of the method, we consider the simple case where all the dislocations have the same Burgers vector \mathbf{b} which is also in the xy plane. The local grain boundary energy in Eq. (24) in this

case is,

$$E_{\text{local}} = \int_{\Gamma} \gamma ds, \quad (\text{A.1})$$

$$\gamma = \frac{\mu b^2}{4\pi(1-\nu)} |\rho| \log \frac{1}{r_g |\rho|}, \quad (\text{A.2})$$

using the dislocation density per unit length ρ .

The variation with respect to the change of Γ is taken under the conservation of the constituent dislocations. Assuming that there is a small change in the location of the grain boundary Γ in its normal direction \mathbf{n} , denoted by $\delta r \mathbf{n}$, the change of energy is

$$\delta E_{\text{local}} = \delta \left(\int_{\Gamma} \gamma ds \right) = \int_{\Gamma} \delta(\gamma) ds + \int_{\Gamma} \gamma \delta(ds). \quad (\text{A.3})$$

In the classical theory of motion by curvature (Herring, 1951; Mullins, 1956; Sutton and Balluffi, 1995), it has been shown that the change of a small arclength ds is

$$\delta(ds) = -\kappa \delta r ds, \quad (\text{A.4})$$

where κ is the curvature of the grain boundary.

For the small arclength ds , the total number of dislocations along ds is $|\rho|ds$. (Note: Using the dislocation density potential function η , it is $d\eta = |\rho|ds$, which is very convenient in the derivation in three dimensions (Zhu and Xiang, 2014).) Conservation of the constituent dislocations gives

$$\delta(|\rho|ds) = \delta|\rho|ds + |\rho|\delta(ds) = 0. \quad (\text{A.5})$$

Further using Eq. (A.4), we have $\delta|\rho|ds + |\rho|(-\kappa \delta r ds) = 0$, or

$$\delta|\rho| = \kappa|\rho|\delta r. \quad (\text{A.6})$$

Using the energy density formula in Eq. (A.2), it can be calculated that

$$\delta(\gamma) = \frac{d\gamma}{d|\rho|} \delta|\rho| = \frac{d\gamma}{d|\rho|} \kappa|\rho|\delta r. \quad (\text{A.7})$$

Substituting Eqs. (A.4) and (A.7) into Eq. (A.3), we have

$$\delta E_{\text{local}} = - \int_{\Gamma} \kappa \left(\gamma - |\rho| \frac{d\gamma}{d|\rho|} \right) \delta r ds. \quad (\text{A.8})$$

Therefore, we have the variation of the energy with respect to the change of the grain boundary profile:

$$\frac{\delta E_{\text{local}}}{\delta r} = -\kappa \left(\gamma - |\rho| \frac{d\gamma}{d|\rho|} \right) = -\frac{\mu b^2}{4\pi(1-\nu)} \kappa |\rho|. \quad (\text{A.9})$$

This is a special case of the variation obtained in Zhu and Xiang (2014), see Eq. (10) with (12) in Sec. 2.

Therefore, the normal velocity of the grain boundary due to the driving force of the variation of the local grain boundary energy is

$$v_n = -\frac{M_d}{|\rho|} \frac{\delta E_{\text{local}}}{\delta r} = M_d \frac{\mu b^2}{4\pi(1-\nu)} \kappa, \quad (\text{A.10})$$

where M_d is the mobility of the constituent dislocations of the grain boundary. Here a factor $1/|\rho|$ has been included with the dislocation mobility M_d so that the velocity of the grain boundary is consistent with the dynamics of its constituent dislocations (Cahn and Taylor, 2004). This can be seen more explicitly from the full variation formula in Eqs. (10) and (12) with all types of driving forces.

Next we consider the variation of the local grain boundary energy in Eqs. (A.1) and (A.2) with respect to the change of the dislocation density per unit polar angle ϱ on the fixed grain boundary. It is easy to calculate that

$$\frac{\delta E_{\text{local}}}{\delta \varrho} = \frac{d\gamma}{d\varrho}. \quad (\text{A.11})$$

Therefore, the evolution of the dislocation density ϱ on the grain boundary is

$$\varrho_t = -M_t \frac{\delta E_{\text{local}}}{\delta \varrho} = -M_t \frac{d\gamma}{d\varrho}, \quad (\text{A.12})$$

where M_t is the mobility.

Acknowledgments

This work was partially supported by the Hong Kong Research Grants Council General Research Fund 606313.

References

A. Basak and A. Gupta. A two-dimensional study of coupled grain boundary motion using the level set method. *Modell. Simul. Mater. Sci. Eng.*, 22:055022, 2014.

B. A. Bilby. In *Bristol conference report on defects in crystalline materials*, page 123. Physical Society, London, 1955.

J. W. Cahn and J. E. Taylor. A unified approach to motion of grain boundaries, relative tangential translation along grain boundaries, and grain rotation. *Acta Mater.*, 52:4887–4898, 2004.

J. W. Cahn, Y. Mishin, and A. Suzuki. Duality of dislocation content of grain boundaries. *Philos. Mag.*, 86:3965–3980, 2006a.

J. W. Cahn, Y. Mishin, and A. Suzuki. Coupling grain boundary motion to shear deformation. *Acta Mater.*, 54:4953–4975, 2006b.

L. Q. Chen and W. Yang. Computer simulation of the domain dynamics of a quenched system with a large number of nonconserved order parameters: The grain-growth kinetics. *Phys. Rev. B*, 50:15752–15756, 1994.

M. Elsey, S. Esedoglu, and P. Smereka. Diffusion generated motion for grain growth in two and three dimensions. *J. Comput. Phys.*, 228:8015–8033, 2009.

S. Esedoglu. Grain size distribution under simultaneous grain boundary migration and grain rotation in two dimensions. *Comput. Mater. Sci.*, 121:209–216, 2016.

F. C. Frank. The resultant content of dislocations in an arbitrary intercrystalline boundary. In *Symposium on the plastic deformation of crystalline solids*, pages 150–154. Office of Naval Research, Pittsburgh, 1950.

T. Gorkaya, D. A. Molodov, and G. Gottstein. Stress-driven migration of symmetrical $<100>$ tilt grain boundaries in al bicrystals. *Acta Mater.*, 57:5396–5405, 2009.

K. E. Harris, V. V. Singh, and A. H. King. Grain rotation in thin films of gold. *Acta Mater.*, 46:2623 – 2633, 1998.

C. Herring. Surface tension as a motivation for sintering. In W. E. Kingston, editor, *The Physics of Powder Metallurgy*, pages 143–179. McGraw-Hill, New York, 1951.

J. P. Hirth and J. Lothe. *Theory of Dislocations*. Wiley, New York, second edition, 1982.

A. Kazaryan, Y. Wang, S. A. Dregia, and B. R. Patton. Generalized phase-field model for computer simulation of grain growth in anisotropic systems. *Phys. Rev. B*, 61:14275–14278, 2000.

D. M. Kirch, E. Jannat, L. A. Barrales-Mora, D. A. Molodov, and G. Gottstein. Inclination dependence of grain boundary energy and its impact on the faceting and kinetics of tilt grain boundaries in aluminum. *Acta Mater.*, 56:4998–5011, 2006.

R. Kobayashi, J. A. Warren, and W. C. Carter. A continuum model of grain boundaries. *Phys. D*, 140: 141–150, 2000.

E. A. Lazar, R. D. MacPherson, and D. J. Srolovitz. A more accurate two-dimensional grain growth algorithm. *Acta Mater.*, 58:364–372, 2010.

C. H. Li, E. H. Edwards, J. Washburn, and E. R. Parker. Stress-induced movement of crystal boundaries. *Acta Metall.*, 1:223–229, 1953.

J. C. M. Li. Possibility of subgrain rotation during recrystallization. *J. Appl. Phys.*, 33:2958–2965, 1962.

A. T. Lim, D. J. Srolovitz, and M. Haataja. Low-angle grain boundary migration in the presence of extrinsic dislocations. *Acta Mater.*, 57:5013–5022, 2009.

A. T. Lim, M. Haataja, W. Cai, and D. J. Srolovitz. Stress-driven migration of simple low-angle mixed grain boundaries. *Acta Mater.*, 60:1395–1407, 2012.

K. McReynolds, K. A Wu, and P. Voorhees. Grain growth and grain translation in crystals. *Acta Mater.*, 120:264–272, 2016.

D. A. Molodov, V. A. Ivanov, and G. Gottstein. Low angle tilt boundary migration coupled to shear deformation. *Acta Mater.*, 55:1843–1848, 2007.

W. Mullins. Two-dimensional motion of idealized grain boundaries. *J. Appl. Phys.*, 27:900–904, 1956.

S. S. Quek, Y. Xiang, and D. J. Srolovitz. Loss of interface coherency around a misfitting spherical inclusion. *Acta Mater.*, 59:5398–5410, 2011.

W. T. Read and W. Shockley. Dislocation models of crystal grain boundaries. *Phys. Rev.*, 75:275–289, 1950.

A. Sidi and M. Israeli. Quadrature methods for periodic singular and weakly singular fredholm integral equations. *J. Sci. Comput.*, 3:201–231, 1988.

S. G. Srinivasan and J. W. Cahn. Challenging some free-energy reduction criteria for grain growth. In S. Ankem, C. S. Pande, I. Ovid'ko, and S. Ranganathan, editors, *Science and Technology of Interfaces*, pages 3–14. TMS, Seattle, 2002.

A.P. Sutton and R.W. Balluffi. *Interfaces in Crystalline Materials*. Clarendon Press, Oxford, 1995.

J. E. Taylor and J. W. Cahn. Shape accommodation of a rotating embedded crystal via a new variational formulation. *Interfaces and Free Boundaries*, 9:493–512, 2007.

S. L. Thomas, K. T. Chen, J. Han, P. K. Purohit, and D. J. Srolovitz. Reconciling grain growth and shear-coupled grain boundary migration. *preprint*, 2017.

Z. T. Trautt and Y. Mishin. Grain boundary migration and grain rotation studied by molecular dynamics. *Acta Mater.*, 60:2407–2424, 2012.

M. Upmanyu, R. W. Smith, and D. J. Srolovitz. Atomistic simulation of curvature driven grain boundary migration. *Interface Sci.*, 6:41–58, 1998.

M. Upmanyu, G. N. Hassold, A. Kazaryan, E. A. Holm, Y. Wang, B. Patton, and D. J. Srolovitz. Boundary mobility and energy anisotropy effects on microstructural evolution during grain growth. *Interface Sci.*, 10:201–216, 2002.

M. Upmanyu, D. J. Srolovitz, A. E. Lobkovsky, J. A. Warren, and W. C. Carter. Simultaneous grain boundary migration and grain rotation. *Acta Mater.*, 54:1707–1719, 2006.

K. A. Wu and P. W. Voorhees. Phase field crystal simulations of nanocrystalline grain growth in two dimensions. *Acta Mater.*, 60:407–419, 2012.

Y. Xiang and X. D. Yan. Stability of dislocation networks of low angle grain boundaries using a continuum energy formulation. *Dis. Cont. Dyn. Sys. B*, doi:10.3934/dcdsb.2017183, 2017.

Y. Xiang, L. T. Cheng, D. J. Srolovitz, and W. E. A level set method for dislocation dynamics. *Acta Mater.*, 51:5499–5518, 2003.

A. Yamanaka, K. McReynold, and P. W. Voorhees. Phase field crystal simulation of grain boundary motion, grain rotation and dislocation reactions in a bcc bicrystal. *Acta Mater.*, 133:160–171, 2017.

H. Zhang, M. Upmanyu, and D.J. Srolovitz. Curvature driven grain boundary migration in aluminum: molecular dynamics simulations. *Acta Mater.*, 53:79–86, 2005.

L. C. Zhang, Y. J. Gu, and Y. Xiang. Energy of low angle grain boundaries based on continuum dislocation structure. *Acta Mater.*, 126:11–24, 2017a.

L. C. Zhang, J. Han, Y. Xiang, and D. J. Srolovitz. The equation of motion for a grain boundary. *preprint*, 2017b.

X. H. Zhu and Y. Xiang. Continuum model for dislocation dynamics in a slip plane. *Philos. Mag.*, 90: 4409–4428, 2010.

X. H. Zhu and Y. Xiang. Continuum framework for dislocation structure, energy and dynamics of dislocation arrays and low angle grain boundaries. *J. Mech. Phys. Solids*, 69:175 – 194, 2014.